# HEAT AS A TRACER TO EXAMINE FLOW IN THE STREAMBED OF A LARGE, GRAVEL-BED RIVER

Matthew H. Silver
B.A., Whitman College, Walla Walla, 2002

THESIS

Submitted in partial satisfaction of
the requirements for the degree of

MASTER OF SCIENCE

in

Geology

at

CALIFORNIA STATE UNIVERSITY, SACRAMENTO

FALL
2007

HEAT AS A TRACER TO EXAMINE FLOW IN THE STREAMBED OF A LARGE, GRAVEL-BED RIVER

A Thesis

by

Matthew H. Silver

Approved by:

_____, Committee Chair
Timothy C. Horner

_____, Second Reader
David G. Evans

_____, Third Reader
James E. Constantz, U.S. Geological Survey

Date:_____

Student: Matthew H. Silver

I certify that this student has met the requirements for format contained in the University format manual, and that this thesis is suitable for shelving in the Library and credit is to be awarded for the thesis.

_____ _____

Timothy C. Horner, Graduate Program Coordinator Date
Department of Geology

Abstract

of

HEAT AS A TRACER TO EXAMINE FLOW IN THE STREAMBED OF A LARGE, GRAVEL-BED RIVER

by

Matthew H. Silver

Shallow temperature profiles were collected in the streambed of a large, gravel-bed river, to estimate seepage and hydraulic conductivity in salmonid spawning habitat. Temperatures and subsurface pressure measurements were modeled to trace the movement of heat and water through the streambed and estimate sediment hydraulic conductivity. Sensitivity analysis shows the highest model sensitivity to hydraulic conductivity, of all model parameters. Vertical-dimension modeling over a 1.2-m domain produces close simulated-observed temperature fits in many cases. Best-fit hydraulic conductivity is apparently higher at shallower depths in the streambed, suggesting a decrease in hydraulic conductivity with depth or diverging subsurface flowpaths. Although this method is applied successfully in areas with downward vertical hydraulic gradients, the vertical-dimension model fails to accurately simulate temperatures at a site with an upward vertical gradient. To evaluate this inconsistency, the influence of longitudinal flow was also examined. Longitudinal flow is shown to account for phase lags in vertically-simulated temperatures. While longitudinal heat transport may be negligible in some cases (downward flow), it does exist and should be incorporated into the method of using heat to trace flow in the shallow streambed, especially when considering upward flow. This study demonstrates that heat is a useful tracer to estimate seepage and hydraulic conductivity in the shallow streambed.

_____, Committee Chair
Timothy C. Horner

# ACKNOWLEDGEMENTS

Advising from Dr. Timothy Horner and Dr. David Evans was invaluable in guiding my work on this thesis. I sincerely thank them for their help toward completing this thesis. In addition to the thesis, I will carry the benefits of learning from them into my future endeavors. I am also grateful to Dr. James Constantz (USGS) for being part of my thesis committee and for helpful conversations regarding my project at several stages. I also thank David Fairman for many days of field assistance; Andrew Head, Tammy Leathers, Mike Lytge, and Bryan Zho, for additional field and laboratory assistance; and Dr. Hedeff Essaid, Celia Zamora, Dr. Rich Niswonger, Dr. Daniel Deocampo, Dr. Kevin Cornwell, Dr. David Ziegler, Dr. Karen Burow, and Dr. Alan Flint, for helpful conversations regarding my project. I am grateful to the US Bureau of Reclamation, for their funding (to Dr. Horner) to study salmonid spawning gravels, and to Geological Society of America, for awarding me a graduate student research grant. Finally, I wish to thank my parents, Frank and Libby Silver, for their all-around support of my efforts in graduate school.

TABLE OF CONTENTS

Page

LIST OF FIGURES

LIST OF TABLES

# Chapter 1

# INTRODUCTION

Naturally-occurring variations in heat have been used to estimate seepage and hydraulic conductivity in porous media beneath streams and other bodies of surface water (Ronan et al., 1998; Constantz et al., 2002; Bravo et al., 2002; Constantz et al., 2003; Su et al., 2004; Anderson, 2005). This is typically accomplished by modeling the coupled flow of water and transport of heat, using numerical solutions to the ground water flow equation and heat transport equation (e.g., Ronan et al., 1998). Water flow parameters (seepage and hydraulic conductivity) have been estimated by calibrating the model to observed temperatures. Uncertainty in parameter estimates have been evaluated through analysis of sensitivity of simulated temperatures to unknown parameters (e.g., porosity, dispersivity, heat capacity; Niswonger and Prudic, 2003). Seepage estimates are produced directly from simulation of heat transport while hydraulic conductivity estimates also depend on flow boundary conditions. While the most common approach is to couple water flow and heat transport, using numerical approximations of the governing equations, some researchers have taken different approaches. Bundschuh (1993) quantified annual amplitude and phase difference in temperature series and used Fourier analysis to calculate flow velocities. Keery et al. (2007) used dynamic harmonic regression to develop an analytical solution to calculate water fluxes from temperature signals collected in shallow vertical profiles, beneath a small stream.

Heat is useful as a tracer in saturated porous media because of changes in temperature that are present at the Earth's surface. Potentially useful fluctuations in temperature occur on daily, weekly, and annual timescales. Daily temperature changes (diurnal fluctuation) have been used to trace water movement in the subsurface (Ronan et al., 1998, Contantz et al., 2002). Diurnal temperature changes typically extend 0.1 m to 10 m into the subsurface, depending on the rate and direction of seepage through the porous medium (Constantz et al., 2003). "Weekly" is used here to refer to any fluctuations on time scales greater than a day but less than a year. A combination of weekly and annual changes in temperature were used by Su et al. (2004), Bravo et al. (2002), and Burow et al. (2005) for model calibration. Annual changes in temperature (seasonal fluctuation) were used by Taniguchi (1993). In general, as the spatial scale of study increases, so should the temporal scale of fluctuations used to trace flow (Constantz et al., 2003). In studies of ephemeral streams (e.g., Constantz and Thomas, 1996; Constantz et al., 2002; Hoffmann et al., 2003), temperatures are typically measured to depths of two to three meters. In studies of perennial streams (e.g., Lapham, 1989; Bartolino and Niswonger, 1999; Bartolino, 2003; Conlon et al., 2003; Su et al., 2004), temperatures are typically measured to depths on the order of tens of meters. However, Zamora (2006) used heat as a tracer to quantify exchanges across the sediment-water interface using 3-m-deep wells in the lower Merced River, a small, regulated perennial stream. All heat as a tracer studies to date (excluding work in wetlands) have been in the vertical and transverse dimensions, with the most common purpose being to estimate recharge to aquifers (e.g., Constantz and Thomas, 1996; Ronan et al., 1998; Bartolino and

Niswonger, 1999; Stonestrom and Constantz, 2003; Su et al., 2004). While some researchers have applied the method in three dimensions (Bravo et al., 2002, modeling a wetland), none, to our knowledge, have used heat to trace streamflow in a longitudinal-vertical profile over a scale of tens of meters. Additionally, in heat tracer studies of large, perennial streams, shallow flow in the streambed has not been the focus of investigations.

Shallow flow is our focus here in order to apply the heat tracer method to evaluation of salmonid spawning habitat. Salmonids generally lay embryos in the upper 30 cm of the streambed. Estimating seepage and hydraulic conductivity has implications for the quality of habitat because seepage through gravel supplies oxygen to eggs (Pollard, 1955), increasing their chances of survival (Sowden and Power, 1985). Larger particles generally allow faster seepage, but fish generally cannot move particles larger than a tenth of their body length; for Chinook salmon and Steelhead trout, this means particles of diameter 2-5 cm are the ideal size of sediment for spawning (Kondolf and Wolman, 1993). Excess fine sediment reduces dissolved oxygen, resulting in lower embryo survival rates (Turnpenny and Williams, 1980). Many environmental factors continue to affect embryos after they emerge, resulting in varied growth rates of juvenile fish (Williams, 2006).

# Chapter 2

# PURPOSE AND OBJECTIVES

The purpose of this paper is to evaluate the potential to use naturally-occurring variations in temperature from shallow vertical temperature profiles to estimate seepage and hydraulic conductivity in a large, gravel-bed stream. This type of environment has yet to be examined using heat as a tracer to characterize shallow flow in the streambed. We focus on shallow flow in attempt to apply the heat tracer method to evaluating salmonid spawning habitat in the lower American River, near Sacramento, California. Compared to recharge studies, the spatial scale of interest in our study is different in two ways: 1) only flow in the shallow streambed directly affects spawning salmonids and 2) longitudinal flow, which may have little importance and consequence when using heat as a tracer to estimate recharge, is important with respect to habitat and characterizing flow in the localized area of interest. Modeling heat as a tracer is a potentially valuable tool for evaluating salmonid spawning habitat, for two reasons: 1) collecting temperature and hydraulic head data requires less disturbance of sensitive salmon spawning habitat, compared to injected tracers, and 2) naturally-occurring variations in heat can provide information over the duration of an entire spawning season, thus accounting for flow patterns over a longer timescale than injected tracers (Constantz et al., 2003).

We will evaluate the potential use of heat as a tracer to evaluate flow in the streambed of a large stream by collecting temperatures in shallow (1.2-m deep) profiles in the streambed and then modeling coupled water flow and heat transport in the vertical

dimension. We seek to determine both seepage and hydraulic conductivity, and thus monitor both streambed temperature and hydraulic gradient. Estimations of seepage have less uncertainty because they do not depend on flow boundary conditions, but quantifying hydraulic conductivity is useful as a characterization of the sediment present in spawning habitat. We will further evaluate application of the technique by analyzing effects of longitudinal flow. Longitudinal flow is a hydrologic issue that has not been emphasized in previous use of heat as a tracer beneath streams.

# Chapter 3

# HYDROLOGIC SETTING AND EXPERIMENTAL DESIGN

## *Lower American River*

The American River is the second largest stream draining the northern Sierra Nevada. Its flow is impeded at Folsom Dam, as it reaches California's Central Valley. The lower stretch of the river (Figure 1) lies on an alluvial fan, formed from transport of sediment out of the Sierra Nevada. The streambed is poorly sorted, with sediment sizes that range from silt to cobbles. An average of 30,000 Chinook salmon spawn in the lower American River annually (Williams, 2001). The reach is also habitat to historically large but rapidly declining populations of Steelhead trout (McEwan, 2001). Upstream migration of salmonids is impeded at Nimbus Dam. Reservoir operations at Nimbus Dam and Folsom Dam control discharge in the lower American River, which typically ranges between 1,500 cfs and 30,000 cfs annually. Flows during fall Chinook spawning

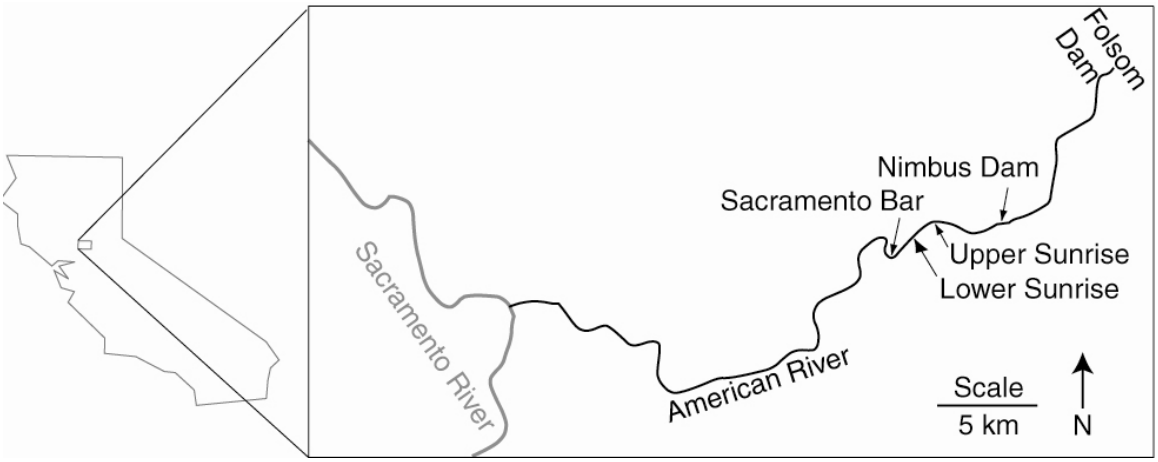


Figure 1. Map showing location of the lower American River, and our field sites.

(October – January) are fairly constant and near the low end of the annual range (1,500 cfs – 3,000 cfs), but are higher and more variable during Steelhead spawning (December – March). A levee system of design capacity 130,000 cfs is present along much of the reach.

Characterizing conditions in spawning habitat is important for restoration efforts. In a nearby a regulated river, gravel restoration is shown to have improved conditions favorable to spawning, such as surface water velocity, streambed permeability, and streambed dissolved oxygen content (Merz and Setka, 2004). In the lower American River, physical conditions in spawning habitat were evaluated by Vyverberg et al. (1997), who concluded that sediment permeability was the most important factor affecting spawning use. Gravel was added to the streambed in 1999 at several sites, including Lower Sunrise and Sacramento Bar (Figure 1). Horner et al. (2003) conducted post-augmentation evaluation and found that permeability still varied greatly at sites where gravel was added. While the gravel component of the streambed is conducive to spawning habitat, gravel tends to be associated with non-Darcian flow conditions. However, sand and silt are present in the interstices of the gravel and should result in Darcian flow conditions in the porous medium. Nevertheless, the gravel component of the lower American River streambed is reason to consider the applicability of a Darcian approach.

*Applicability of a Darcian Approach*

Most previous studies that used heat as a tracer have been conducted in streambeds containing sand and smaller-sized sediment, and Darcian flow is assumed.

Use of a Darcian approach to modeling heat transport (i.e., coupling heat transport with ground water flow) requires that Darcian flow conditions are present in the streambed. We estimated values of Reynolds number ($R$), to evaluate the applicability of a Darcian approach in the coarser gravel material of the lower American River. The Reynolds number is calculated by

$$R = \rho q d/\mu,$$

where $\rho$ is density, $q$ is darcy velocity, $d$ is pore diameter, and $\mu$ is viscosity. Fluid density and viscosity vary with temperature; we assumed values based on temperatures of 7°C and 17°C, corresponding to the annual range in field conditions. We also collected field data from a riffle to estimate pore diameter and Darcy velocity. Surface water velocity is relatively high in riffles, so if turbulent flow is present in the streambed, it would occur here. We collected sediment freeze cores to estimate pore diameter, from depths of 10 cm – 60 cm in the streambed. All cores showed silt and sand filling the space between cobbles. The upper 10 cm of the streambed did not freeze, so we inspected it visually. The same pattern of finer sediment (sand and silt) filling space between cobbles was present in the surficial material. This suggests that flow through the streambed is slower than would be expected for a streambed made solely of cobbles. Pore diameter is sometimes estimated from a $D_{50}$ (50%-finer diameter) or $D_{10}$ (10%-finer diameter) value, taken from a cumulative frequency distribution curve. We chose to use the $D_{10}$, because finer sediment will control the size of the pore space. $D_{10}$ from our freeze cores in the riffle was $8 \times 10^{-3}$ m (8 mm). Water velocity through the porous medium was estimated

using a chloride tracer test in the riffle, conducted over a scale of 1.5 m. Assuming 25% porosity, we obtained a darcy velocity of $7.5 \times 10^{-4}$ m/s.

Using these values, we obtained Reynolds numbers of $4 \leq R \leq 6$. Darcian conditions in the subsurface are thought to exist when Reynolds numbers are less than about 1 to 10 (Bear, 1972). Although the value we calculated is within the range of the upper limit of acceptable values for Darcian flow, the riffle site chosen is likely to have the highest Reynolds number (based on high surface water velocity) of all sites considered. In other studies with some similarities in field conditions, Ronan et al. (1998) use a Darcian approach in a streambed containing some gravel, while Constantz et al. (2002) did the same to analyze infiltration from periodic, high-energy flows in an ephemeral channel. Thus, while we cannot unequivocally say that Darcian conditions exist, there is adequate reason based on success of previous studies and assessment of our field conditions to use a Darcian approach to heat as a tracer.

*Temperature and Pressure Data*

Vertical temperature profiles were collected at each site by installing 3.9-cm inner-diameter PVC pipe in the streambed, similar to the method described by Su et al. (2004). However, we measured pressure next to the casing used for temperature sensors, so the casing was sealed on the bottom, rather than screened. The pipes were capped on the top, to prevent stream water from entering after the pipe initially filled with water. Constantz et al. (2002) showed that temperatures collected in this manner are very similar to temperatures measured in the streambed, outside the casing. Data-logging thermistors (Onset Hobo Water Temp Pro) were then suspended on a string, inside the pipe. The

sensors were installed at depths of 0 m, 0.30 m, 0.60 m, and 1.20 m beneath the sediment-water interface. In most cases, data were collected every 15 minutes for the duration of monitoring at each site. Vertical temperature profiles were collected in three areas of the river (Figure 1): Upper Sunrise, Lower Sunrise (shown in detail in Figure 2), and Sacramento Bar.

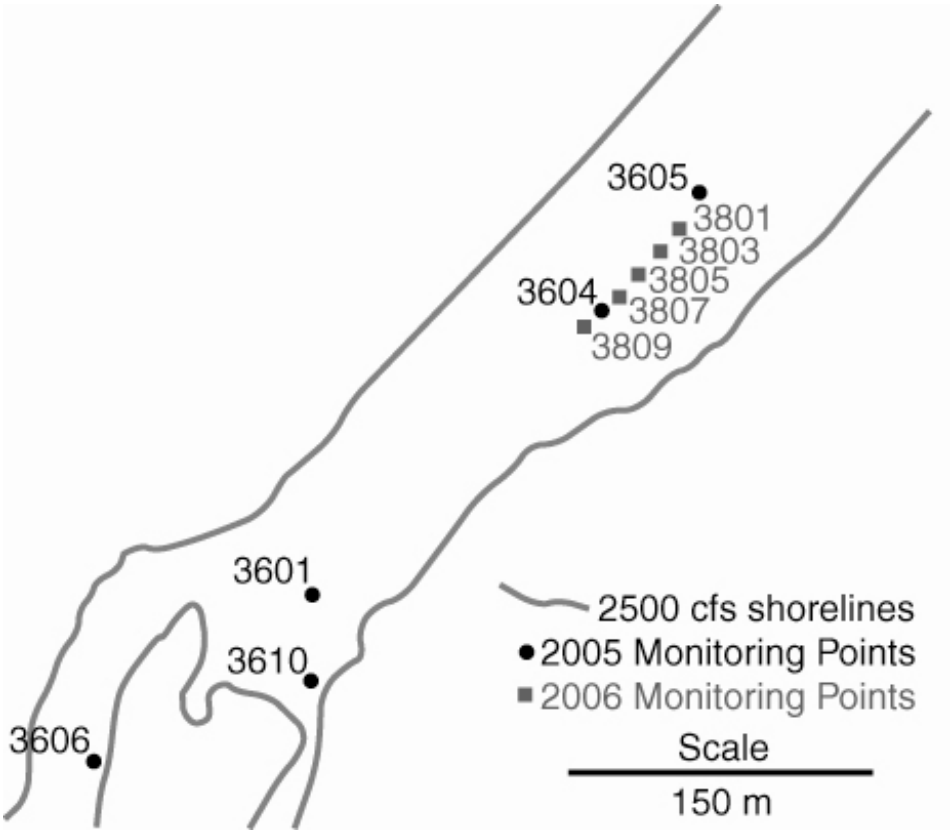


Figure 2. Subsurface temperature monitoring sites at Lower Sunrise.

We used mini-piezometers and a bubble manometer board to measure subsurface pressure conditions next to each temperature monitoring site (Figure 3). Mini-piezometers were fashioned from 2-cm-long steel tips containing a small screened portion, attached to the surface with a plastic tube (Lee and Cherry, 1978). The tips were

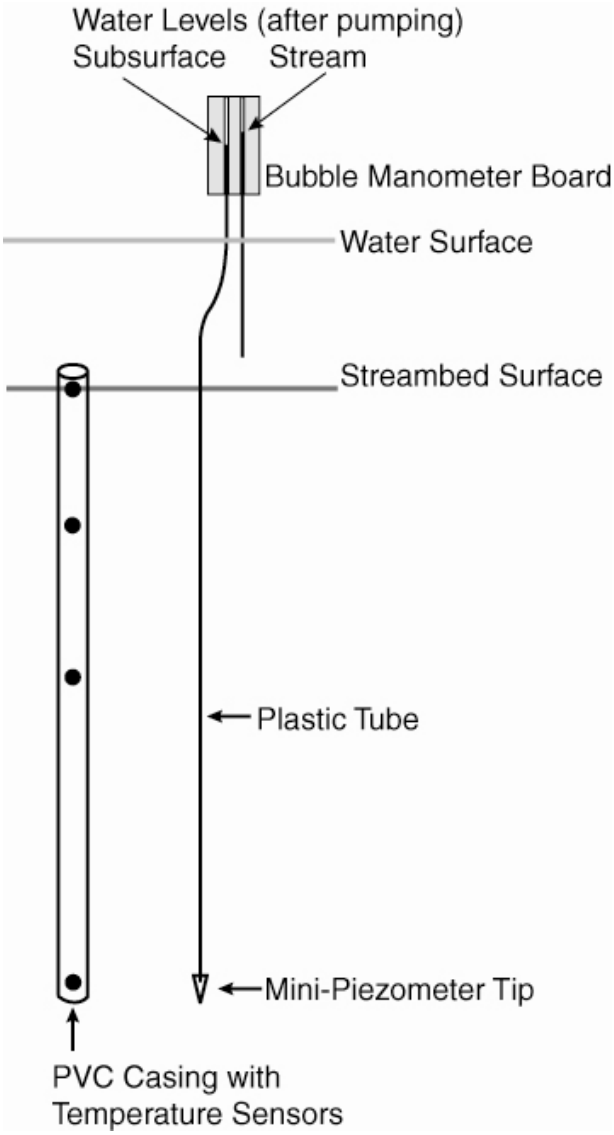


Figure 3. Field instrumentation used to collect temperature and pressure data.

manually driven 1.20 m into the streambed and then developed by pumping until water appearance changed from silt-filled to clear. To take a measurement of subsurface-to-surface pressure difference, we connected one chamber of a bubble manometer board to the mini-piezometer and the other to the stream. We then pumped until water from both sources was bubble-free, sealed the chamber, and read the difference in the two water

levels on the manometer board. Where subsurface pressure was higher than stream pressure, the pressure difference was assigned a negative value; where stream pressure was higher than subsurface pressure, the pressure difference was assigned a positive value. Vertical hydraulic gradient was then calculated by dividing the pressure difference by the distance from the gravel surface to the mini-piezometer (1.2 m). Pressure differences measured using mini-piezometers are listed in Table 1. Discharge from Nimbus dam (Nimbus release) values are from California Data Exchange Center, available online at cdec.water.ca.gov.

| Site | Date | Nimbus Release (cfs) | Pressure Difference (m) | Vertical Hydraulic Gradient (m/m) |
|---|---|---|---|---|
| 2601 | 9/29/2005 | 2600 | -0.30 | -0.25 |
| 3601 | 9/29/2005 | 2600 | -0.081 | -0.068 |
| | 11/18/2005 | 2300 | -0.083 | -0.069 |
| 3606 | 9/23/2005 | 2500 | 0.008 | 0.007 |
| 3610 | 8/9/2005 | 3600 | -0.12 | -0.10 |
| | 8/19/2005 | 3000 | -0.16 | -0.14 |
| 5605 | 9/25/2005 | 3000 | -0.032 | -0.027 |
| 5606 | 9/25/2005 | 3000 | -0.008 | -0.0067 |

**Table 1**. Pressure differences measured with mini-piezometers.

*Theory of Heat Transport in Saturated Porous Media*

The advection-conduction equation (heat transport equation) governs the transport of heat in saturated, homogeneous porous media. In recent use of heat as a tracer, some researchers include a dispersion coefficient ($D_h$) to the second derivative (Laplacian) term

(Ronan et al., 1998; Constantz et al., 2002). The constant-fluid-density form of the heat transport equation (with dispersion) is

$$(D_h + \kappa_e)\nabla^2 T - C_w \nabla(q \cdot T) = C' \frac{\partial T}{\partial t}$$

where $D_h$ is the thermomechanical dispersion tensor (Healy and Ronan, 1996), $\kappa_e$ is the effective thermal conductivity of water and sediment, $C_w$ is volumetric heat capacity of water, $q$ is specific discharge, and $C'$ is effective volumetric heat capacity of water and sediment. Many researchers (e.g., Smith and Chapman, 1983, Ronan et al., 1998, Constantz et al., 2002, Su et al., 2004) suggest thermal dispersivities are significant and include the thermomechanical dispersion tensor as a term multiplying the second derivatives, while others (e.g., Bravo et al., 2002, Keery et al, 2007) argue that dispersivity is negligible. Hopmans et al. (2002) show that dispersivity is increasingly important at higher water flow velocities. Because surface water moves relatively quickly at our sites and because the streambed contains poorly sorted sediment, indicating potential for considerable variation in subsurface flow pathways and travel times, we will consider dispersivity as a variable affecting heat transport.

Because energy must be conserved, reducing a heat transport problem to fewer than three dimensions requires that terms in the dimensions not considered are negligible. However, if a horizontal temperature gradient is present, there must be some (albeit possibly negligible) horizontal heat transport. Temperature fluctuations are large at the sediment-water interface and attenuate with depth (Lapham, 1989, Silliman and Booth, 1993). Because the most appreciable differences in temperature in the shallow subsurface

of the streambed are from heat moving vertically, we begin by modeling heat transport in the vertical dimension only.

Estimating hydraulic conductivity through heat transport modeling was proposed by Stallman (1965) and later applied with use of numerical techniques (e.g., Woodbury and Smith, 1988; Lapham, 1989, Constantz et al., 2002, Su et al., 2004). However, hydraulic conductivity is not a variable in the heat transport equation. Heat transport is coupled to the ground water flow equation through the darcy velocity ($q$) term. Coupling heat transport with water flow requires boundary conditions for both processes. Water fluxes are produced from flow variables (including hydraulic conductivity) and boundary conditions (hydraulic head) and then used, through the heat transport equation, to simulate temperatures within the model domain.

Constantz and Stonestrom (2003) used conceptual temperature-depth profiles to show that when minimum (daily or annual) temperature is present at the surface, geotherms increase with depth. When maximum (daily or annual) temperature is present at the surface, geotherms decrease with depth. We will use the annual cases of these geotherms to refer to thermal conditions, on time scales greater than one day, as "wintertime" if the surface temperature is cooler, and "summertime" if the surface temperature is warmer.

*Modeling Methods*

Suzuki (1960) proposed using the advection-conduction equation to calculate infiltration from vertical temperatures. Analytical solutions were formulated by Stallman (1965), through analysis of the attenuation of daily temperature fluctuations with depth,

and by Bredehoeft and Papadopulos (1965), using temperature-depth type curves. Lapham (1989) solved Suzuki's (1960) equation numerically. Numerical solutions have been widely used in the last decade (e.g., Ronan et al., 1998; Bartolino and Niswonger, 1999; Constantz et al., 2002; Su et al., 2004), with many researchers using the USGS program VS2DH (Healy and Ronan, 1996). Our simulations were performed in VS2DHI (Hsieh et al., 2000), a graphical program based on VS2DH. VS2DH uses finite differences to approximate values of derivatives in governing equations for flow (ground water flow equation) and transport (heat transport equation).

To construct vertical models, we used an L x 1 m domain, where L is the measured distance between the uppermost and lowermost temperature sensors and 1 m is the unit width (Figure 4). A grid of at least 100 rows was used in all simulations. Observation points were set at the measured depths of temperature sensors located within the domain. Depending on the number of temperature sensors deployed at the field site, either one or two observed temperature series were available for comparison to simulated temperatures. A single, homogenous textural class was assigned for each simulation, consisting of sediment and transport properties. The first objective in modeling was to investigate the sensitivity of the model to variations in unknown parameters. The second objective was to adjust parameters, particularly vertical hydraulic conductivity ($K_z$), until the best possible match was obtained. The modeling process proceeded by running the forward model and then comparing the simulated temperature to the observed temperature series at fixed observation points.

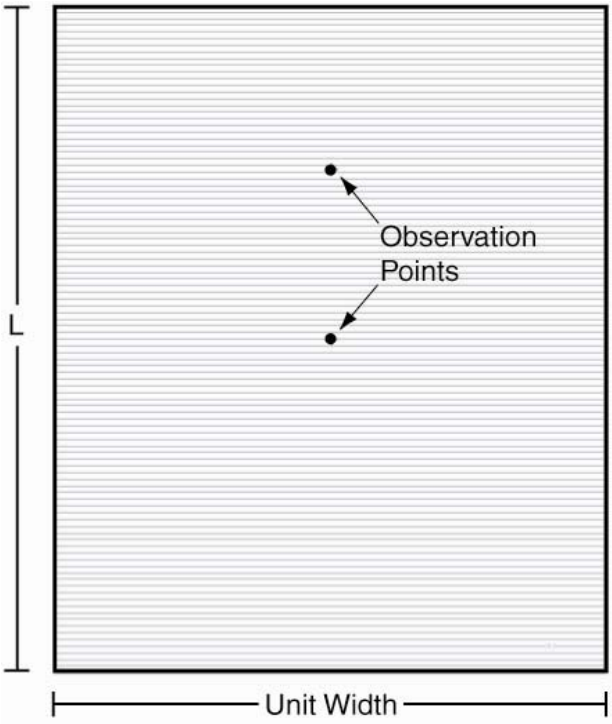


Figure 4. Model domain, observation points, and finite-difference grid constructed for simulations.

*Initial and Boundary Conditions*

Two boundaries are present in the one-dimensional model. The upper and lower boundaries were assigned a total head condition for flow and a temperature condition for heat transport. Time series data from the uppermost and lowermost temperature sensors in the monitoring pipe were use for the temperature (heat transport) boundary conditions. The boundary condition for flow was defined as steady-state (constant) values for total head. Total head at the upper boundary was calculated as $Z_{UB} + d_{water}$, where $Z_{UB}$ is the elevation of the upper boundary above an arbitrary datum and $d_{water}$ is the water depth, measured at the monitoring site. Total head at the lower boundary was calculated as $Z_{LB} + L + d_{water} - h_{diff}$, where $Z_{LB}$ is the elevation of the lower boundary above the arbitrary

datum and $h_{diff}$ is the measured pressure difference. Initial conditions were set in grid cells adjacent to the upper and lower boundaries and varied linearly from top to bottom. Values assigned for temperature were measurements taken immediately before the modeled time period. Values assigned for flow were the same as the total head assigned in the boundary conditions.

Although the sediment-water interface represents a real boundary, the depth of the deepest temperature sensor does not correspond to any known physical boundary. We conducted a series of numerical experiments using VS2DH to determine if temperatures collected at an arbitrary subsurface depth may be used as a proxy for boundary conditions. In step one, synthetic data generated using sine functions were assigned as boundary conditions of head and temperature, at depths of 0 m and 2 m below the sediment-water interface. These were used to perform forward simulations, with output generated at nodes located 0.3 m, 0.6 m, and 1.2 m below the upper boundary. Step two was an inverse problem, with temperature series output in step one at the lower (1.2 m) node used as the transport boundary condition. Using this new arbitrary boundary, temperatures were simulated at nodes located 0.3 m and 0.6 m below the top of the domain. We could then compare, at each of these two output nodes, the simulated temperatures from steps one and two. This process allowed us to assess whether the arbitrary nature of the lower boundary affects simulated temperatures.

Simulations were run for ten sets of synthetic boundary conditions. Amplitude and surface-subsurface temperature difference were varied when generating sets of boundary conditions. The temperature range chosen generally corresponded to

temperatures seen in profiles collected in the field. In all cases, the temperature series simulated in the forward problem matched the temperature series simulated in the inverse problem, at both (0.3 m and 0.6 m) simulation nodes. Because the same temperatures were produced using each of the arbitrary lower boundaries, the depth where lower boundary temperatures are measured does not affect simulated temperatures. We thus conclude that temperatures measured at an arbitrary depth in the subsurface may reasonably be used as a proxy for boundary conditions.

# Chapter 4

# MODEL RESULTS

## *Model Fit*

Vertical modeling was performed with time-series vertical temperature profiles. Both the observed and simulated temperatures were viewed as periodic, oscillating signals. To evaluate the fit of model results, we considered four signal characteristics: 1) phase (arrival time of daily minimum and maximum temperature), 2) amplitude (difference between daily minimum and maximum temperature), 3) mean value (value of daily minimum and maximum temperature), and 4) temperature trend on time scales greater than one day (weekly trend). These characteristics are similar to Bundschuh's (1993) use of annual amplitude and phase difference, while Su et al. (2004) use root-mean-square (RMS) difference. We quantified the goodness of fit using mean phase difference ($\Delta\varphi$) and root-mean-square difference, normalized to the range of observed temperatures ($RMS_{norm}$). The former allowed us to look in detail at the specific signal characteristic of phase, while the latter provided an overall indication of goodness of fit. Phase difference was calculated from the time of the simulated daily maximum temperature ($\varphi_{sim}$) and observed daily maximum temperature ($\varphi_{obs}$):

$$\Delta\varphi = \frac{\sum_{i=1:N} \varphi_{sim} - \varphi_{obs}}{N},$$

where $N$ is number of days. Daily maximum temperature was used because daily maxima are more distinct in the observed temperatures than daily minima. RMS difference

normalized to range in observed temperature is calculated as from observed temperature ($T_i$), simulated temperature ($U_i$), maximum temperature in the observed signal ($T_{MAX}$), and minimum temperature in the observed signal ($T_{MIN}$):

$$RMS_{norm} = \sqrt{\frac{\sum_{i=1:M} (\tau_i - \upsilon_i)^2}{M}},$$

where $\tau_i = (T_{MAX} - T_i)/(T_{MAX} - T_{MIN})$, $\upsilon_i = (T_{MAX} - U_i)/(T_{MAX} - T_{MIN})$, and M is number of discrete time periods in the temperature series. $RMS_{norm}$ is more appropriate than conventional RMS difference because the temperature range (daily amplitude and differences due to weekly trend) in the shallow streambed varied greatly by depth and site. Conventional RMS difference is not a function of any characteristic of the observed signal, while $RMS_{norm}$ reflects the simulated-observed difference relative to the overall range in observed temperature.

*Sensitivity to Model Parameters*

Simulations were performed for site 3601 to analyze the sensitivity of simulated temperature series to variation in unknown parameters used in modeling. Temperatures were simulated at 30 cm depth. Niswonger and Prudic (2003) identified unknown parameters used in water flow and heat transport modeling and classified sensitivity of results to each as “high”, “moderate”, or “low”. Of parameters included in fully-saturated, one-dimensional modeling, five were classified as high or moderate: hydraulic conductivity, porosity, dispersivity, sediment heat capacity, and effective thermal conductivity. While these general sensitivities are known, it is important to evaluate the sensitivities using the data collected for our study. Thus, the sensitivity of simulated

temperatures to these five parameters was investigated using a range of values for each. Our largest data set is at site 3601, so this site was chosen for a detailed sensitivity analysis.

We first examined sensitivity to vertical hydraulic conductivity ($K_z$). For 1 m/d ($1.2 \times 10^{-5}$ m/s) $\leq K_z \leq$ 70 m/d ($8.1 \times 10^{-4}$ m/s), variations in the amplitude and phase of simulated temperatures were large (Figure 5). In general, a higher $K_z$ resulted in greater amplitude and earlier phase. For $K_z \geq$ 70 m/d, however, the changes were less dramatic. The same general effects on amplitude and phase remain, but the changes in amplitude and phase are not as large. Model results were thus very sensitive to $K_z$ for 1 m/d $\leq K_z \leq$ 70 m/d, but less sensitive for $K_z \geq$ 70 m/d. It should be noted, however, that when viewing simulation results from sites with different pressure gradients, the $K_z$ range

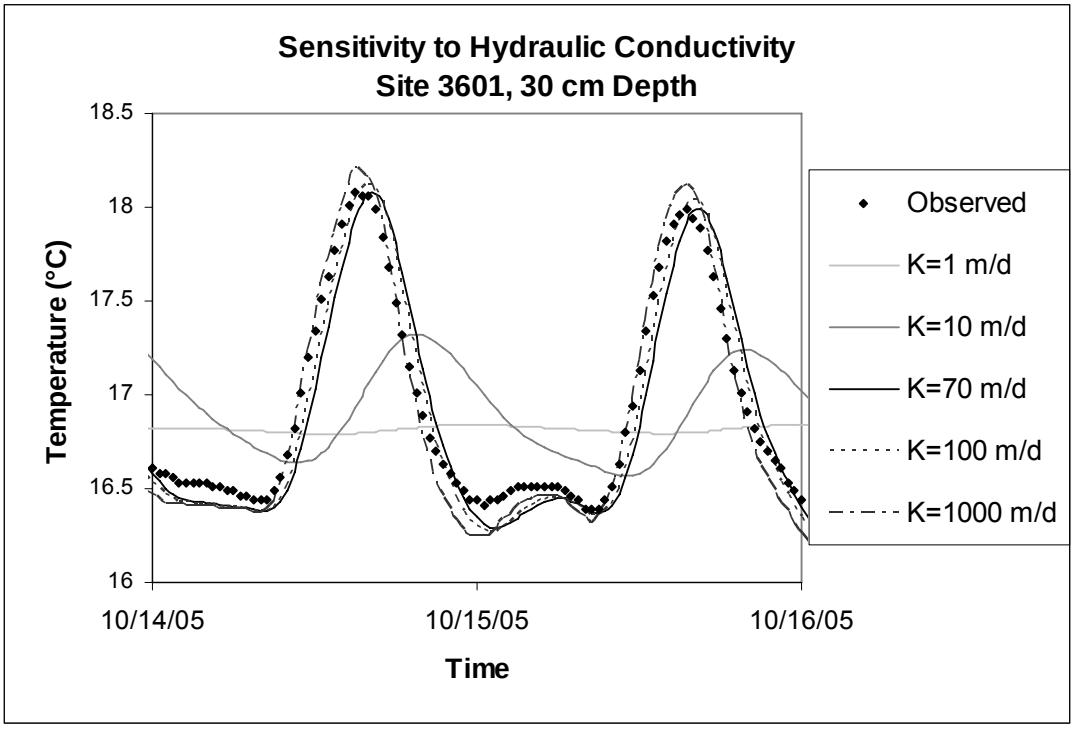


Figure 5. Sensitivity of simulated temperatures to hydraulic conductivity.

where sensitivity of simulated temperatures is greatest will likely be different. Through Darcy's law, $K_z$ is directly proportional to $q_z$, the latter of which is a term in the heat transport equation. Under different pressure conditions, hydraulic gradient will be different. We thus expect the range of high sensitivity to $K_z$ to be a function of hydraulic gradient, making the sensitivity range site- and time-specific.

Parameters resulting in the best simulated-observed match were $K_z \geq 70$ m/day, porosity ($n$) = 0.3, dispersivity ($\alpha$) = 0.12, sediment heat capacity ($C_s$) = 1.2 x $10^6$ J/m$^3$°C, and effective thermal conductivity ($\kappa_e$) = 1.8 (W/m°C)[3]. Once these values had been used to fit the curve, we examined remaining parameters individually, varying only one of the above values at a time. Thermal dispersivity in sediments is typically between 0.01 m and 0.5 m (Constantz et al, 2003). Lower dispersivity resulted in higher amplitude of diurnal fluctuation and earlier phase (Figure 6). Porosity typically ranges from 0.25 to 0.40 in streambed sediments (Niswonger and Prudic, 2003) but may be as low as 0.2 in a sandy gravel (Fetter, 1994). Changes in simulated temperature due to different values of porosity are low, with a slight increase in amplitude and earlier phase at lower porosities (Figure 7). Sediment heat capacity is typically between 1.1 and 1.3 x $10^6$ J/m$^3$°C (Niswonger and Prudic, 2003). Lower heat capacity produced slightly higher amplitude and earlier phase (Figure 8). Temperatures simulated using the range of 1.4 to 2.2 W/m°C (Niswonger and Prudic, 2003) were identical in our sensitivity analysis.

With several unknown variables resulting in different simulated temperatures, solutions are non-unique. However, simulated temperatures for site 3601 are most sensitive to hydraulic conductivity, the variable we seek to estimate, within the range

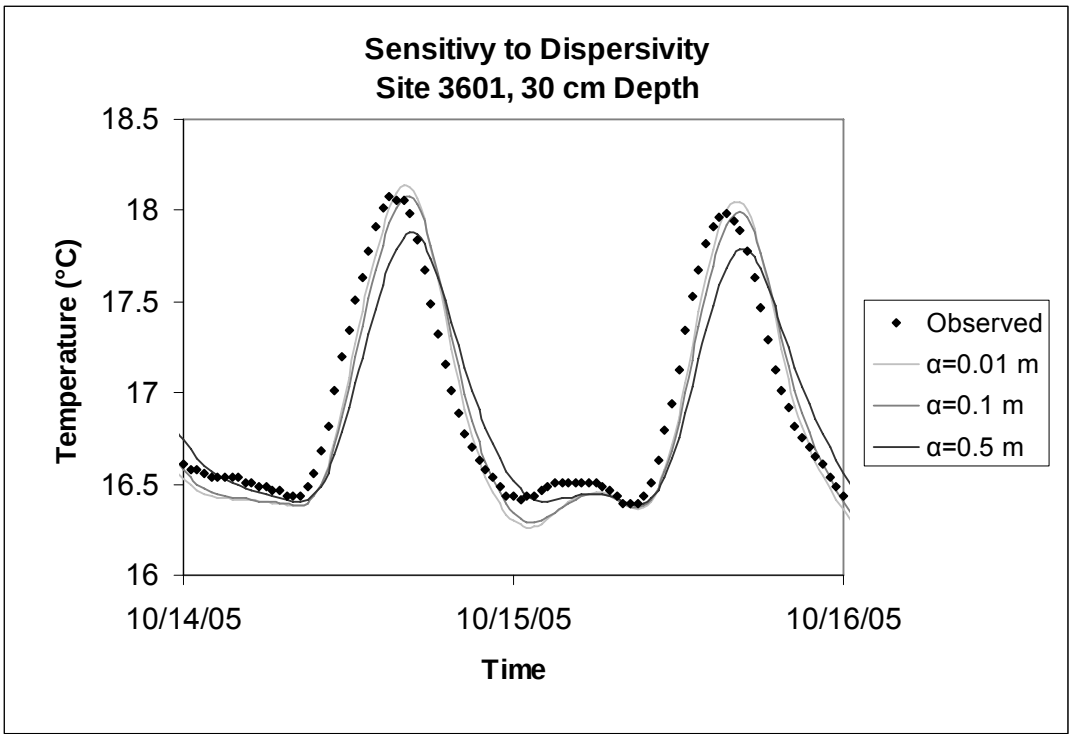


Figure 6. Sensitivity of simulated temperatures to dispersivity.

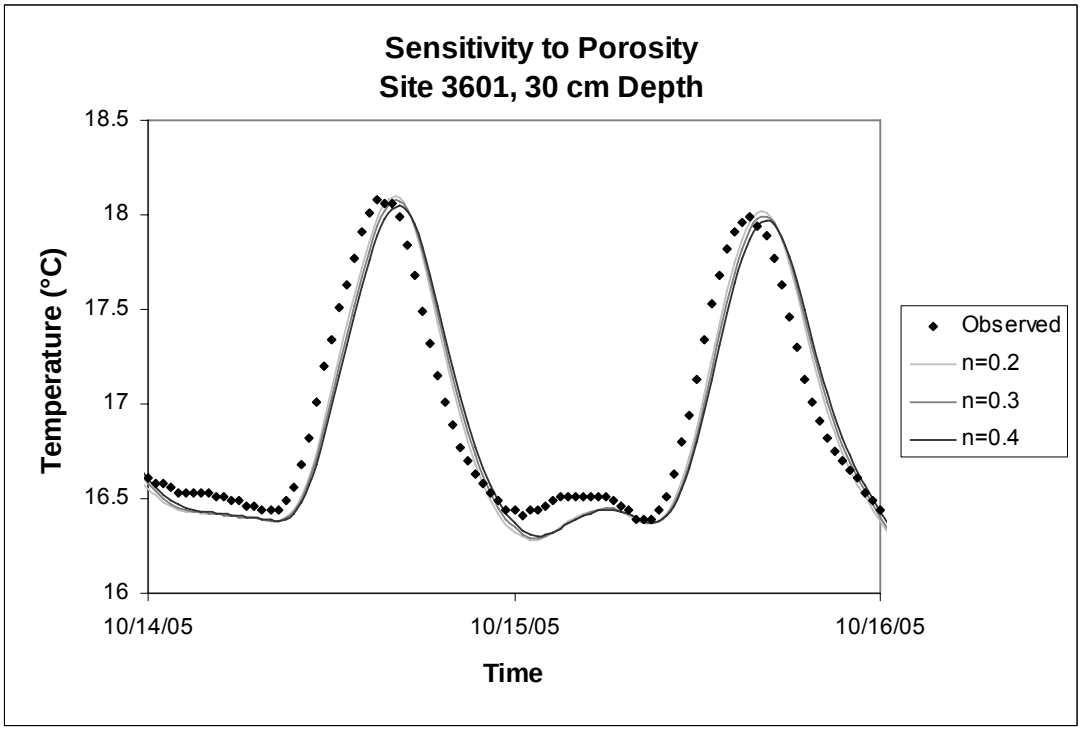


Figure 7. Sensitivity of simulated temperatures to porosity.

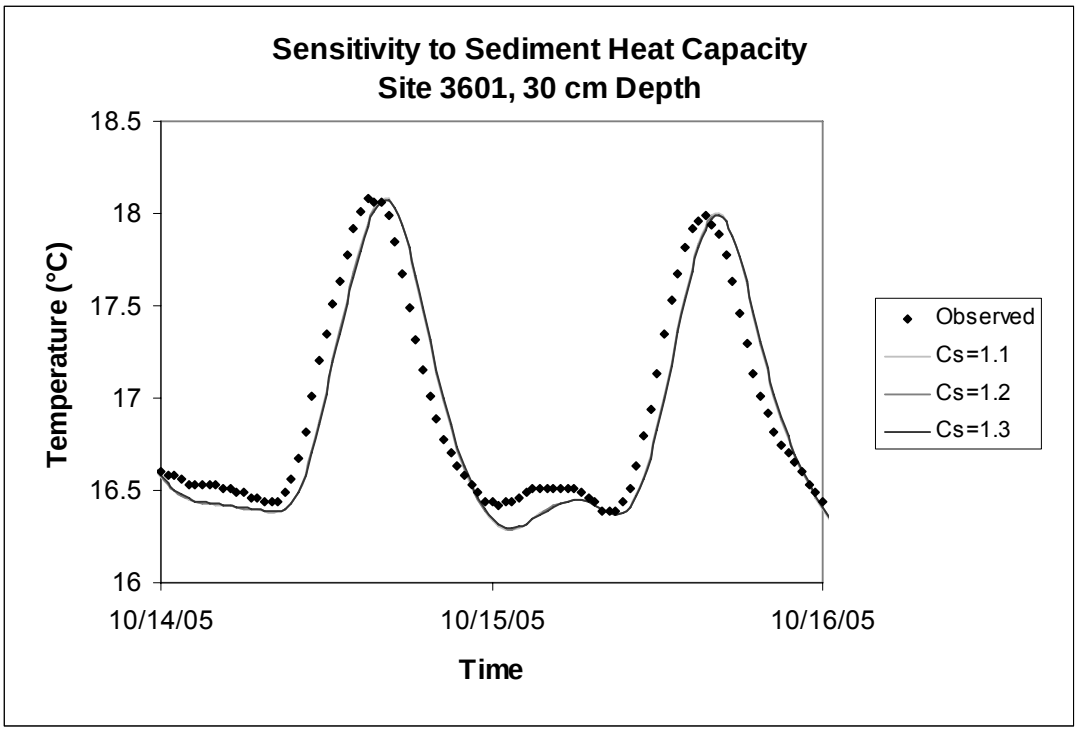


Figure 8. Sensitivity of simulated temperatures to sediment heat capacity. Units of heat capacity are $10^6$ J/$m^3$ °C.

1 m/d $\leq K_z \leq$ 70 m/d. Results are somewhat sensitive to dispersivity, porosity, and sediment heat capacity. Varying dispersivity resulted in small changes in amplitude and phase. Porosity ($n$) and sediment heat capacity ($C_s$) combine to determine effective heat capacity ($C'$), through the equation $C' = nC_w + (1\text{-}n)C_s$. Low porosity together with low sediment heat capacity will thus produce more conductive transport, resulting in earlier phase and higher amplitude. Conversely, high porosity together with high sediment heat capacity will inhibit conductive transport, resulting in later phase and lower amplitude.

*Best-Fit Hydraulic Conductivity: Site 3601*

Conditions at site 3601 were modeled for two time frames: 10/11/2005 through 10/17/2005 (early fall) and 11/19/2005 through 12/17/2005 (late fall). The measured

pressure difference at this site was large (Table 1). River discharge (Q) through each time frame was within 100 cfs of values shown in Table 1, allowing use of constant flow boundary conditions. Simulating early fall temperatures, the best match at the upper (30 cm) observation point (Figure 9) is obtained for $K_z$=70 m/d. The mean value of simulated temperatures is slightly low and phase slightly late, with a normalized RMS difference of 0.11. At the lower observation point (Figure 10), $K_z$ = 10 m/d gives the best match. Even with the best fit, simulated phase is late, with a normalized RMS difference of 0.16. In late fall simulations, slightly lower hydraulic conductivities resulted in the best matches: $K_z$ = 50 m/d at the upper observation point (Figure 11) and $K_z$ = 6 m/day at the lower observation point (Figure 12). In addition to the diurnal fluctuation, the weekly trend is matched well. The matches have normalized RMS differences of 0.02 at the upper observation point and 0.01 at the lower observation points. Values used for other parameters are $\alpha$ = 0.12 m, $n$ = 0.3, and $C_s$ = 1.2 x $10^6$ J/$m^3$°C.

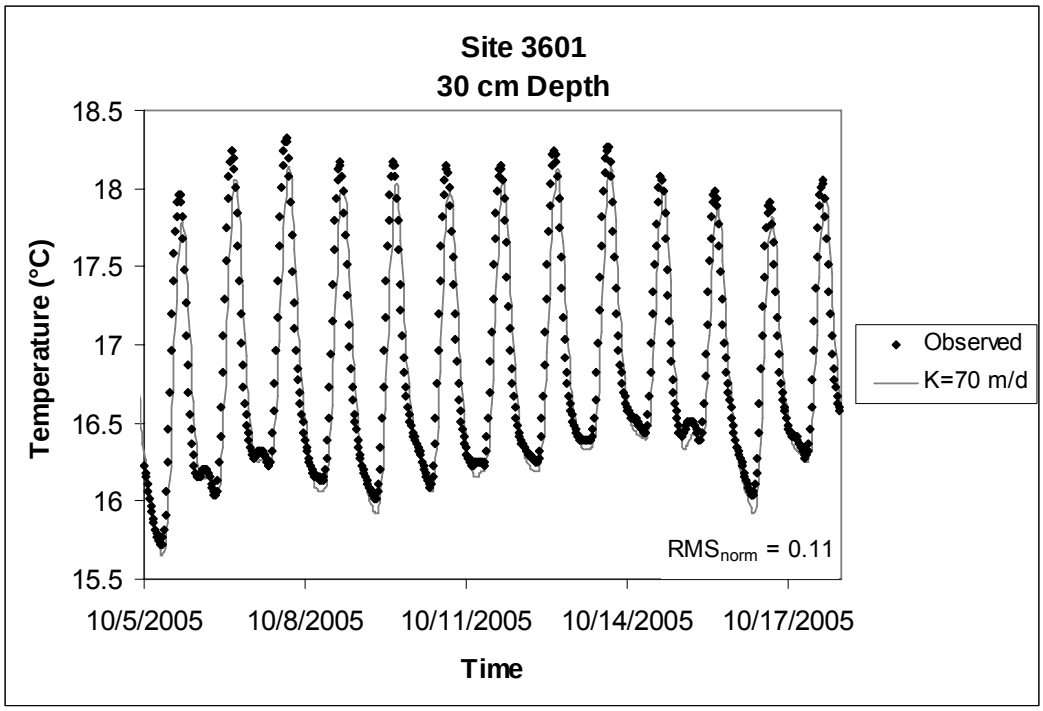


Figure 9. Observed and best-fit simulated temperatures for site 3601, early fall, upper observation point.

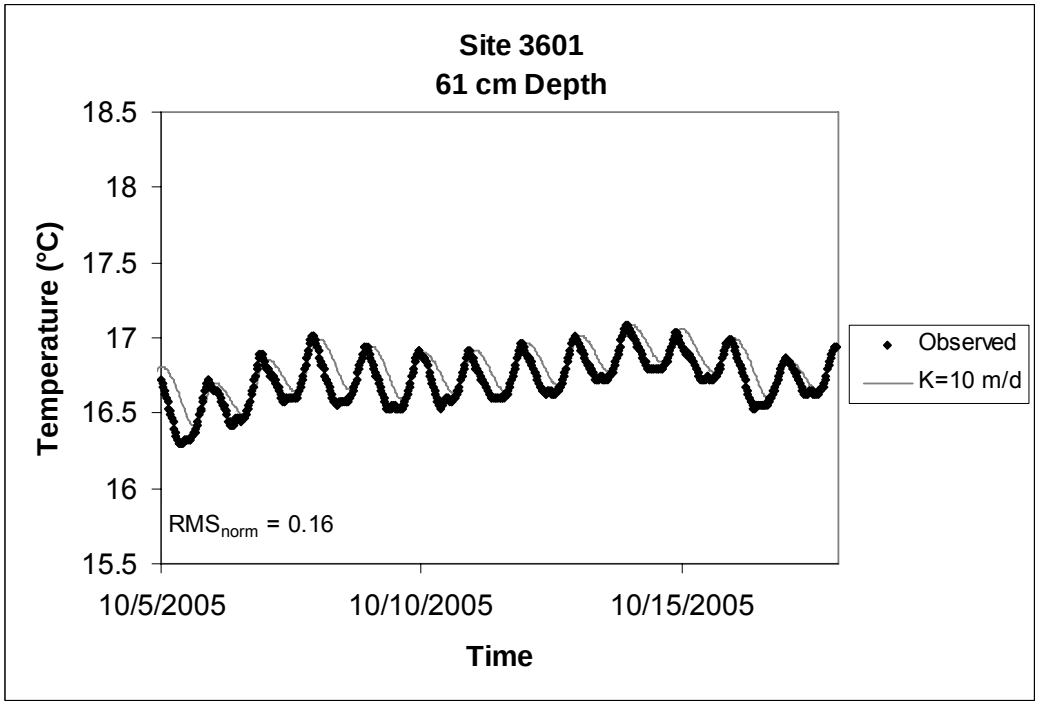


Figure 10. Observed and best-fit simulated temperatures for site 3601, early fall, lower observation point.

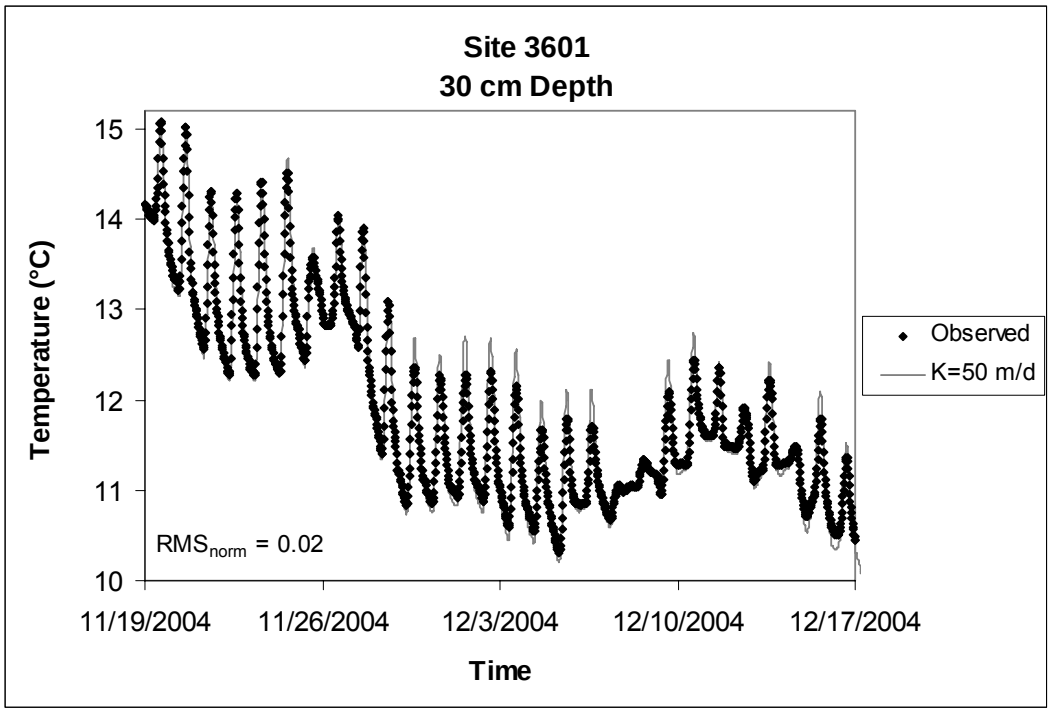


Figure 11. Observed and best-fit simulated temperatures for site 3601, late fall, upper observation point.

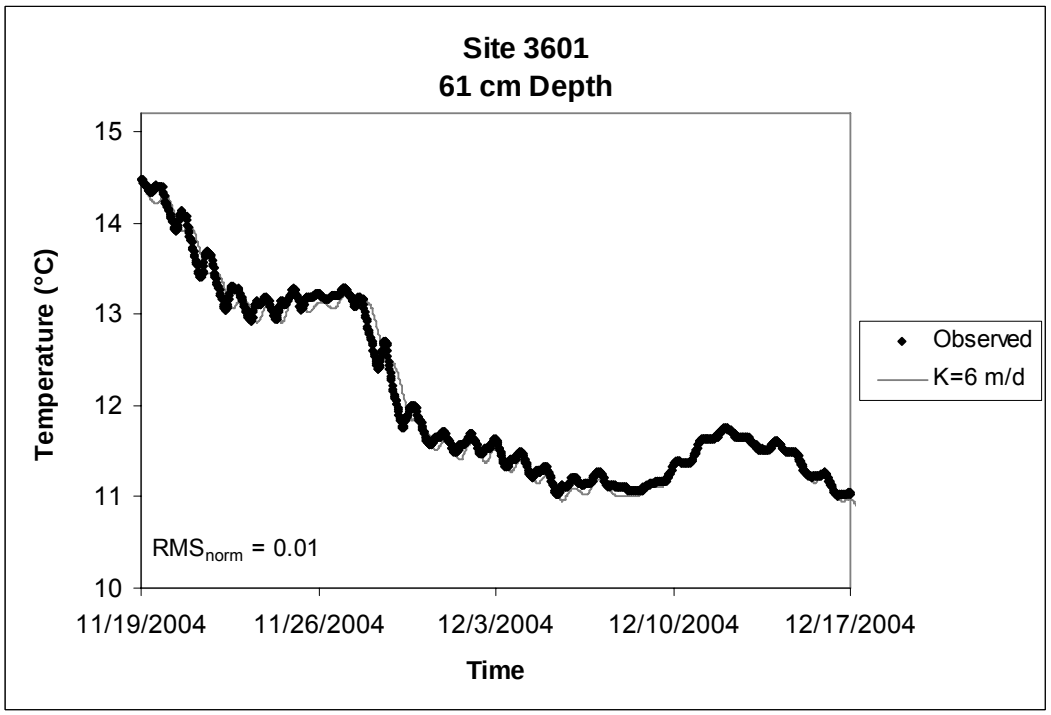


Figure 12. Observed and best-fit simulated temperatures for site 3601, late fall, lower observation point.

*Upward Flow: Site 3606*

The measured pressure difference at site 3606 (Table 1) indicates an upward hydraulic gradient. The site is located on the downstream end of a gravel bar (Figure 2). Simulated temperatures, using several $K_z$ values between 1 m/d and 500 m/d (other parameter values were the same as those noted above), are nearly identical to each other and the observed temperature at the lower boundary (observed to be nearly constant). The observation point temperatures have higher mean value and diurnal fluctuation. Empirically, Silliman and Booth (1993) show that diurnal fluctuations do not penetrate deep into the subsurface in a gaining reach of a stream. In theory, if there is strictly upward flow in the streambed (i.e., no transverse or vertical water movement), advection should only bring constant-temperature water upward, meaning conduction is the only way diurnal fluctuations would penetrate into the streambed.

To determine if these temperatures may be produced by conduction, we changed sediment properties as much as possible within ranges indicated by the literature (Niswonger and Prudic, 2003; Fetter, 1994): $n = 0.2$, $C_s = 1.1 \times 10^6$ J/m$^3$°C, $K_e = 2.2$ (W/m°C). Simulated temperatures at the 30 cm observation point show diurnal fluctuation comparable in amplitude to observed temperatures, but the mean value of simulated temperatures is still too low (Figure 13). Simulated temperatures at the 60 cm observation point also show diurnal fluctuation, but less than observed (Figure 14). The simulated temperature mean value is again lower than observed. These results show that conduction can, to some extent, account for the diurnal fluctuation in the streambed at this site. However, increasing conduction does little to improve the mean value of

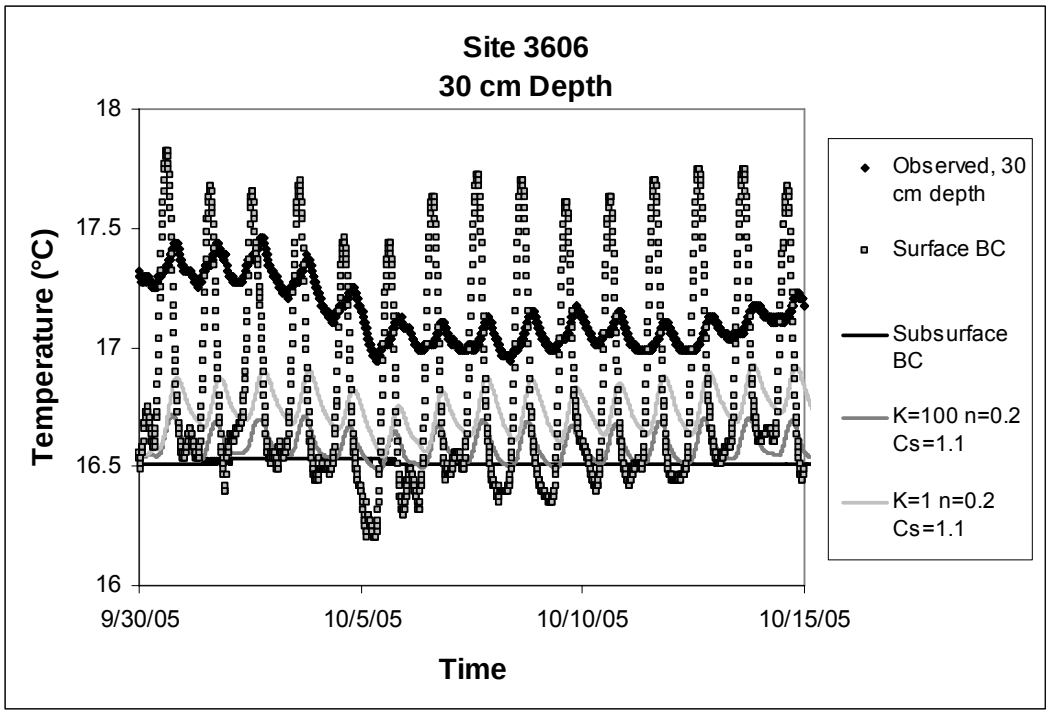


Figure 13. Observed and simulated temperatures at monitoring point 3606, upper observation point, using variables to maximize conduction.

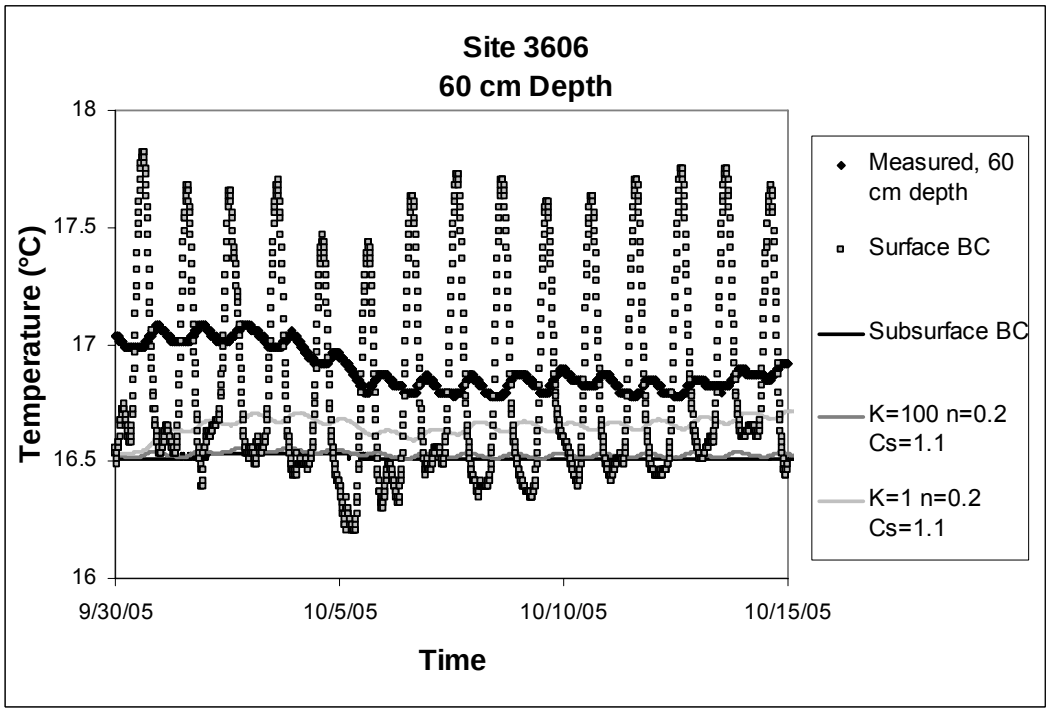


Figure 14. Observed and simulated temperatures at monitoring point 3606, lower observation point, using variables to maximize conduction.

simulated temperatures. Because there is no complete one-dimensional explanation for the difference between simulated and observed temperatures, we suggest that longitudinal flow has affected the observed temperatures in this vertical profile. We did not estimate a value for $K_z$ in this case, because the simulated-observed matches are poor and sensitivity of simulated temperatures to hydraulic conductivity is low.

*Other Sites*

Simulations were performed with data from other sites: site 2601, at Upper Sunrise (Figure 1), site 3610, at Lower Sunrise (Figure 2); and sites 5605 and 5606 at Sacramento Bar (Figure 1). Parameter values used were the same as stated above for site 3601, with the following exceptions: sites 3610 and 5606, $\alpha = 0.5$ m; site 5606, $\alpha = 0.1$ m. These values of dispersivity, in each case, resulted in the closest phase match. Best-fit hydraulic conductivity is higher at the upper observation point, in all cases. Hydraulic conductivity ($K_z$) and volumetric seepage ($q_z$) estimates show variation over two orders of magnitude. In most cases, the phase of simulated temperatures is late (positive $\Delta\varphi$).

| | Upper Observation Point | | | | Lower Observation Point | | | |
|---|---|---|---|---|---|---|---|---|
| Site | $K_z$ (m/d) | $q_z$ (m/d) | RMS-$_{norm}$ | $\Delta\varphi$ (h) | $K_z$ (m/d) | $q_z$ (m/d) | RMS-$_{norm}$ | $\Delta\varphi$ (h) |
| 2601 | 50 | 11 | 0.04 | 0.5 | 15 | 3.3 | 0.10 | 1.8 |
| 3601 early fall | 70 | 4.0 | 0.11 | 1.3 | 10 | 0.57 | 0.16 | 2.8 |
| 3601 late fall | 50 | 2.8 | 0.02 | 0.1 | 6 | 0.34 | 0.01 | 0.5 |
| 3610 | 5 | 0.57 | 0.21 | -1.5* | 3 | 0.34 | 0.35 | 5.5* |
| 5605 | 200 | 3.8 | 0.09 | 1.2 | 30 | 0.58 | 0.22 | 8.6 |
| 5606 | 200 | 0.65 | 0.15 | -0.6 | 50 | 0.16 | 1.1 | -0.1 |

Table 2. Summary of best-fit results from all sites. $RMS_{norm}$ and $\Delta\varphi$ reflect goodness of fit.
*In the temperature signals recorded at site 3610, daily minimum temperatures were used to calculate $\Delta\varphi$, because they were more distinct than daily maxima.

*Discussion*

Simulations presented above suggest that hydraulic conductivity in the lower American River streambed varies spatially. Best-fit $K_z$, at upper observation points, varies between 5 and 200 m/d (Table 3), suggesting lateral variation in hydraulic conductivity. Comparing best-fit $K_z$ between observation points at the same site also suggests spatial variation in hydraulic conductivity: in all cases, best-fit $K_z$ were lower at the lower observation point. Lateral variations in streambed hydraulic conductivity have previously been suggested (e.g., Wroblicky et al., 1998; Landon et al., 2001). The presence of vertical variation in hydraulic conductivity is less well established, but has been suggested in previous work. Landon et al. (2001), working in sandy streams, found lower hydraulic conductivity below 0.3 m, based on grain size distributions and slug tests. Cardenas et al. (2003) show hydraulic conductivity changing with depth, measured through constant-head injection tests, but the trend is not clearly toward lower hydraulic conductivity with depth. Su et al. (2004), using heat as a tracer, obtain improved simulated-observed matches by modeling with a 1-m thick low-conductivity layer in the streambed.

We see three possible reasons for the apparent decrease in hydraulic conductivity at greater depth: 1) compaction of streambed sediments becoming greater, with increasing depth in the streambed, 2) infiltrating fine sediment and organic matter accumulating at depth in the streambed, and 3) patterns of longitudinal flow (not modeled), such as high velocities near the sediment-water interface or flow paths diverging at depth, if present, could create artifacts in results from the simplified (one-

dimensional) model. Chen (2000) suggests compaction of sediment as a reason for anisotropy of hydraulic conductivity, but does not investigate changes in its vertical or horizontal value with depth. Infiltration of fine sediment and organic matter is suggested by Lisle (1989) as a factor affecting sediment in salmonid spawning habitat in several north-coastal California streams. In one freeze core sample taken about 60 m upstream from site 3601, we found a mud-rich layer at 23-41 cm below the sediment-water interface. This freeze core sample and selected previous work on the subject provide some verification of the interpreted decrease in hydraulic conductivity with depth, but only the vertical component of flow was modeled. The lower best-fit hydraulic conductivity at depth may exist physically, or may be an artifact of a simplified model. We now consider the influence of longitudinal flow on heat as a tracer in the shallow streambed.

# Chapter 5

# LONGITUDINAL HEAT TRANSPORT

In the simulations discussed above, we considered heat transport in the vertical ($z$) dimension only. The temperature in vertical profiles, however, also depends on any input (or loss) of heat from both advection and conduction, in the transverse ($y$) and longitudinal ($x$) dimensions. Because the spatial scale defined by the 1.2-m depth of our profiles is small, and because our monitoring sites are in located within a large stream, advective transport in the transverse dimension is assumed to be negligible. The influence of conduction (in any dimension) may be evaluated by estimating the Peclet number ($N_{PE}$). The Peclet number is the ratio of advective to conductive terms in the heat transport equation, along with a scale term:

$$N_{PE} = C_w q L / \kappa_e,$$

where $C_w$ is the heat capacity of water, $q$ is Darcy velocity, $L$ is the length of interest, and $\kappa_e$ is effective thermal conductivity. $N_{PE} > 1$ indicates advection-dominant conditions, $N_{PE} < 1$ indicates conduction-dominant conditions, and $N_{PE}$ near 1 indicates a combination of both. We assumed values of $4.2 \times 10^{6}$ J/m$^3$°C for $C_w$ and 2.2 (W/m°C) for $K_e$. For $q$, we consider the value obtained from the chloride tracer test, $8 \times 10^{-4}$ m/s. When $L = 0.5$ m, $N_{PE} = 760$, indicating advection-dominant conditions. $N_{PE}$ becomes less than one when L is below $7 \times 10^{-4}$ m, indicating that advection is the primary heat transport process at spatial scales larger than this value. At lower velocities and $L = 0.5$ m, $q = 1 \times 10^{-4}$ m/s results in $N_{PE} = 95$ and $q = 5 \times 10^{-6}$ m/s results in $N_{PE} = 5$. Overall, one transport

process (advection or conduction) usually dominates, with permeability being the primary factor determining which heat transfer process dominates (Smith and Chapman, 1983). Based on large Peclet numbers, we conclude that the system is advection-dominated and that conduction terms, in any dimension, may be treated as negligible in most cases.

In the vertical dimension, downward-flowing water brings temperature fluctuations into the subsurface, while fluctuations attenuate quickly with depth where water flows upward (Silliman and Booth, 1993). While this pattern exists for temperature signals in vertical profiles, longitudinal variations in temperature are not as predictable. Cartwright (1974) uses seasonal temperature differences to detect longitudinal ground water flow through a 500-m-long transect. Over a shallower and shorter spatial scale in the streambed, we would expect to see the greatest longitudinal change in temperature where changes in vertical flow exist along a longitudinal transect. Raised bedforms, such as riffles, typically create downward flow at their upstream margins and upward flow at their downstream margins (Thibodeaux and Boyle, 1987). To examine these flow patterns, data were collected in the summer of 2005 at sites 3604 and 3605 (Figure 2), located at the margins of a riffle.

*Numerical Experiments*

In evaluating simulated-observed temperature fits from vertical models, we considered four specific signal characteristics. Of those, amplitude and weekly trend matched well. However, phase generally did not match and in some cases (e.g., site 3606), nor did mean value. Simulated daily peak temperatures were usually late relative

to the observed temperatures (Table 2). Simulated temperatures for site 3606 were lower than observed temperatures at the two observation depths. Heat transport was modeled in the vertical dimension only, and while vertical transport occurs in the shallow streambed, the vertical model is simplified. Specifically, it fails to account for longitudinal heat transport. We hypothesize that both of these inconsistencies (late simulated phase and lower mean value) arise because the phase and mean value of the observation point temperatures are influence by longitudinal heat transport.

We conducted a series of numerical experiments to evaluate the posed hypotheses. Numerical experiments were performed in VS2DH and involved two steps (Figure 15): 1) a forward problem of longitudinal flow through a 75 m x 2 m domain, and 2) an inverse problem with vertical, downward flow in a 1.2 m, unit-width domain at a chosen *x* value within the initial longitudinal domain. Flow in the forward problem was driven by a higher hydraulic head at the upstream (vertically-oriented) boundary, compared to the downstream boundary, with a no-flow condition on the upper and lower

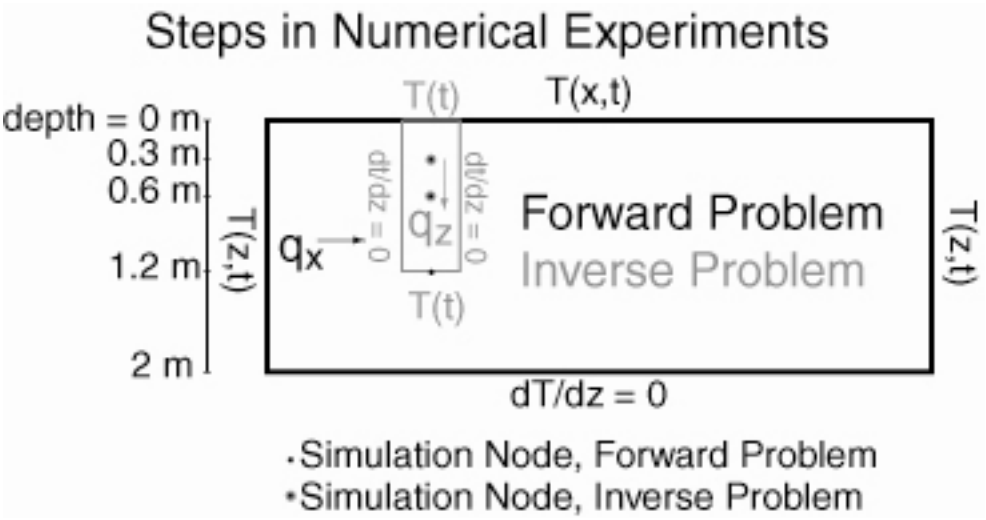


Figure 15. Steps in numerical experiments to investigate longitudinal heat transport.

(horizontally-oriented) boundaries. Flow in the inverse problem was driven by a higher hydraulic head at the upper boundary, compared to the lower boundary, with a no-flow condition on both of the side (vertically-oriented) boundaries.

Boundary conditions for heat transport were assigned from observed temperatures in vertical profiles, collected in July-August 2005 at sites 3604 and 3605 (Figure 2). At the upstream and downstream vertical boundaries, temperatures were assigned according to their measured depths. The upper boundary was broken into 5 m segments and temperatures were assigned by linear interpolation between the upstream and downstream measured temperatures at the sediment-water interface. The lower boundary was assigned a no-energy-flux condition. The upstream temperature profile showed more diurnal fluctuation at all depths, compared to the downstream profile. The same phase is present in the upstream and downstream temperature signals at the sediment-water interface.

Distinct temperature signals resulted from varied flow rates ($q_x$). We simulated temperatures at nodes 30 cm and 60 cm below the upper boundary, and 19 m, 38 m, and 57 m from the upstream boundary. Effects of longitudinal transport were most pronounced at 19 m nodes, with effects becoming slightly less pronounced at the 38 m and 57 m nodes. In general, the amplitude of simulated temperatures is largest closest to the upstream and upper boundaries, and decreases downstream and vertically downward. Simulated temperatures from 19-m downstream nodes are shown in Figure 16 (30 cm deep) and Figure 17 (60 cm deep). For higher flow rates, simulated temperature mean values are higher (summertime conditions) and peak arrivals are earlier.

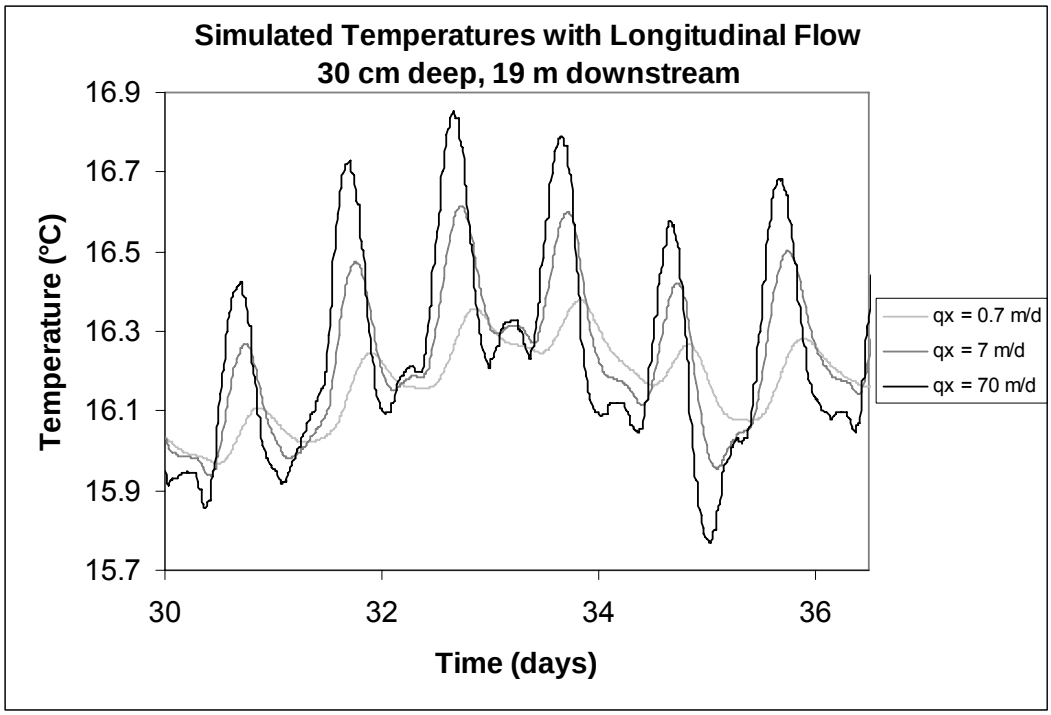


Figure 16. Effects of longitudinal flow rate on simulated temperatures, 30 cm deep and 19 m downstream.

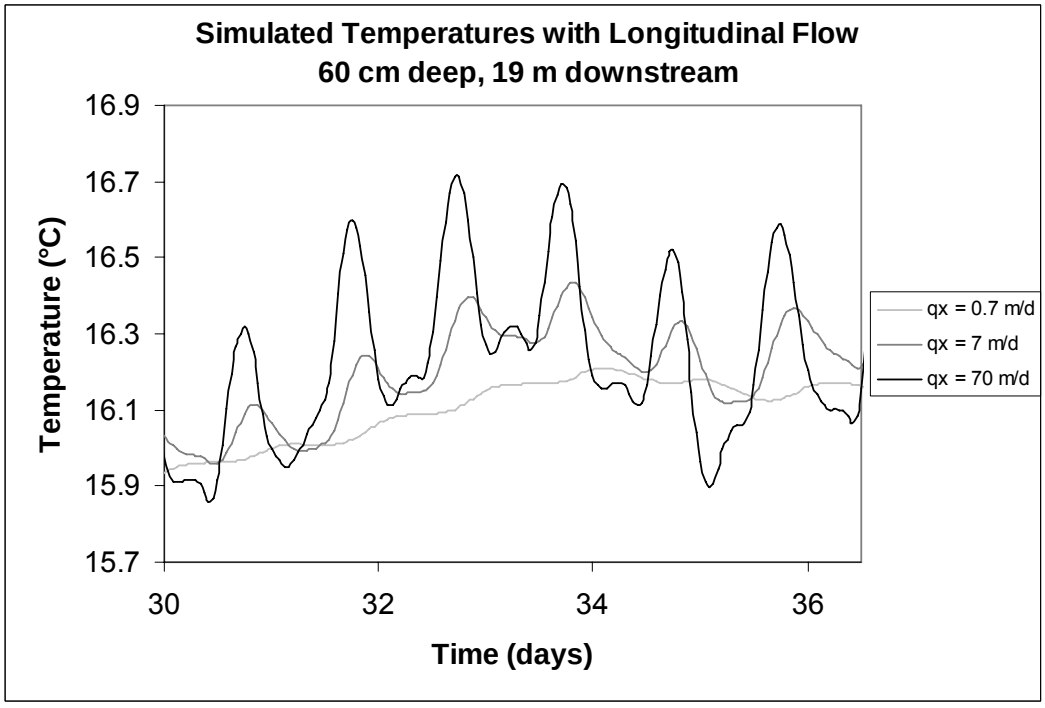


Figure 17. Effects of longitudinal flow rate on simulated temperatures, 60 cm deep and 19 m downstream.

The inverse problem consisted of several repetitions of the following step: a simulated temperature series from a specific simulation node and $q_x$ in the forward problem was chosen to act as a proxy for observed temperatures. We treated temperatures simulated with longitudinal flow (forward problem) as analogous to observed temperatures in earlier vertical-dimension problems, and temperatures simulated with vertical flow (inverse problem) as analogous to simulated temperatures in the earlier vertical models. In each step, we thus follow the procedure of earlier vertical-dimension modeling: we varied $q_z$ until the amplitude matched the forward problem temperatures. Boundary conditions for transport at the upper boundary were the same as the interpolated temperatures used at the upper boundary, at the downstream distance of the inverse problem domain. At the lower boundary, simulated temperatures from 1.2-m deep nodes in forward simulations were used, corresponding to the $q_x$ value we attempt to match to in each sub-step.

These vertical-dimension problems were completed at each of the three downstream distances of simulation nodes in the forward problem. Again, effects were most apparent 19 m downstream from the upstream boundary. Results from three steps are shown, each at 19 m downstream: $q_x$ = 70 m/d at 30 cm depth (Figure 18), $q_x$ = 7 m/d at 30 cm depth (Figure 19), and $q_x$ = 70 m/d at 60 cm depth (Figure 20). In all cases, the phase of the vertically-simulated ($q_z$) temperatures is late, compared to the forward problem ($q_x$) temperatures.

In our earlier vertical-dimension treatment of heat tracer problems, the phase of simulated temperatures was often late. Late arrival of daily maximum and minimum

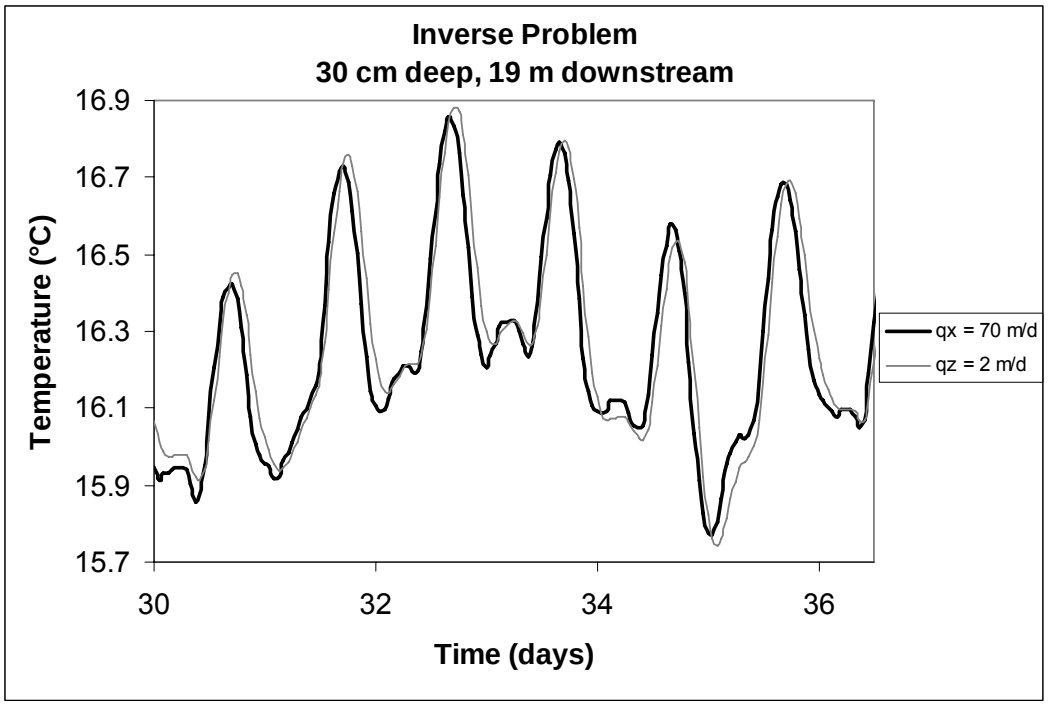


Figure 18. Temperatures simulated to match $q_x$ = 70 m/d, 30 cm deep and 19 m downstream. Vertically-simulated temperatures have later phase.

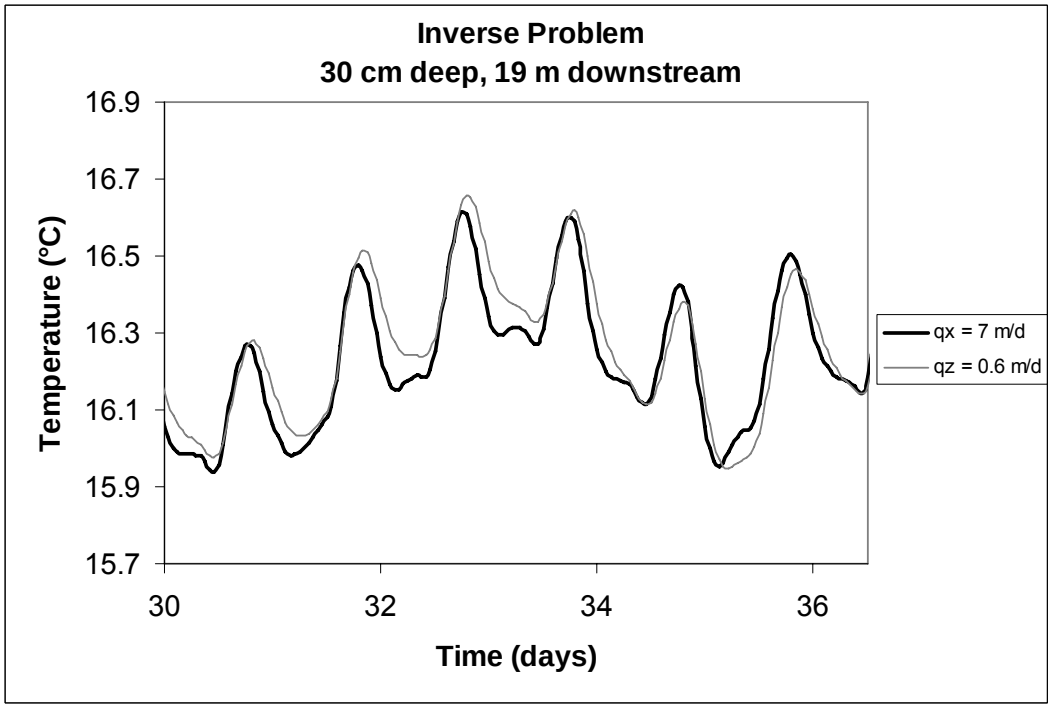


Figure 19. Temperatures simulated to match $q_x$ = 7 m/d, 30 cm deep and 19 m downstream. Vertically-simulated temperatures have later phase.

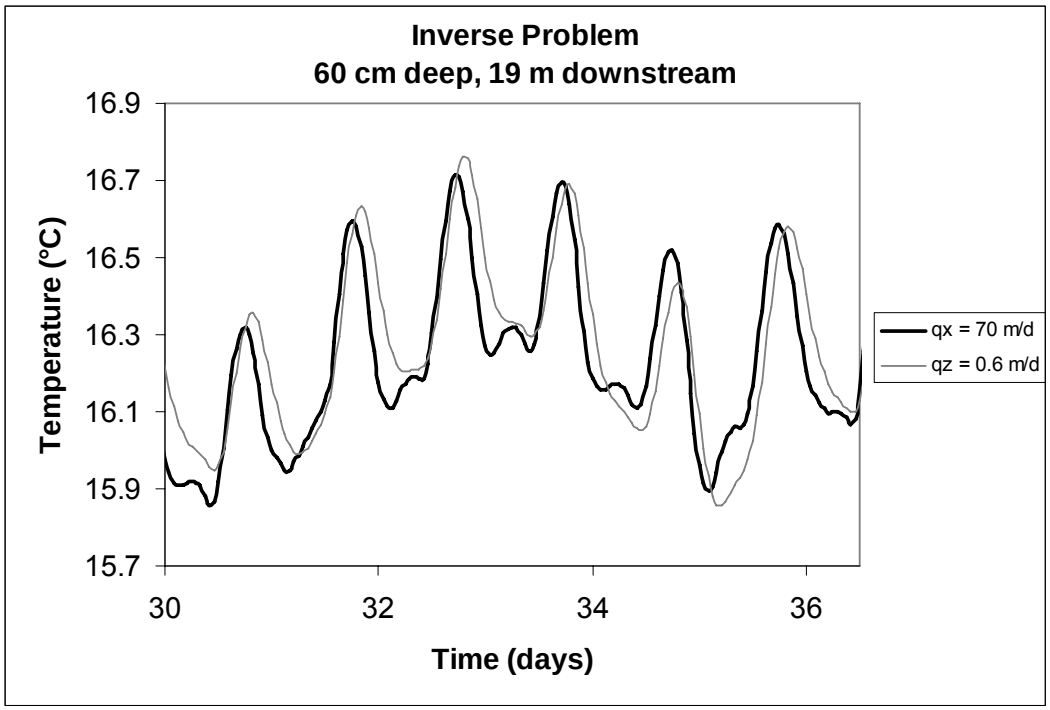


Figure 20. Temperatures simulated to match $q_x$ = 70 m/d, 60 cm deep and 19 m downstream. Vertically-simulated temperatures have later phase.

temperatures (phase) is apparent, to some degree, in all simulations shown earlier at site 3601; it is also common at the other sites shown in Table 3. Failing to account for longitudinal transport provides a reasonable explanation for the late simulated phase. Physically, longitudinal transport may add heat from upstream areas with flow into the streambed, resulting in earlier peak temperatures. We also hypothesized that longitudinal transport may account for lack of match of temperature mean value. In simulations of site 3606 conditions, the simulated temperature mean value was too low. In theory, during summertime conditions, longitudinal flow bringing water from an upstream area with significant flow into the streambed should add heat to the subsurface. Thus, in a vertical profile with an upward component of flow (e.g., site 3606), water flowing in horizontally

from upstream would bring in additional heat. We predicted vertically-simulated temperatures would be lower, compared to the proxy temperature from the forward problem, on the basis of the observed temperatures in earlier vertical problems apparently being raised by longitudinal heat transport. However, the numerical experiments did not verify this prediction.

*Indications of Longitudinal Transport in Observed Temperatures*

Data were collected in a detailed transect through the riffle at Lower Sunrise in the summer of 2006 (sites 3801-3809, Figure 2). Subsurface pressure data were collected along with temperatures, using a movable mini-piezometer during pre-installation reconnaissance and then by installing pressure transducers inside screened PVC pipe. Downward or negligible vertical gradients were measured at sites 3801, 3803, 3805, and 3807; an upward vertical gradient was measured at site 3809. These pressure gradients fit the conceptual model of subsurface flow through a riffle, proposed by Thibodeaux and Boyle (1987). To determine if any longitudinal flow may be inferred from the collected temperatures, temperatures from equal depths in the streambed at sites 3803 (upstream) and 3809 (downstream) are shown (Figure 21, 30 cm depth; Figure 22, 60 cm depth). The downstream temperatures had less diurnal fluctuation and higher wintertime temperatures. These differences could be produced by vertical heat transport alone, or by a combination of vertical and longitudinal transport. However, the phase of weekly fluctuations in temperature is also later at the downstream site. The later arrival of peak temperatures suggests longitudinal advective transport.

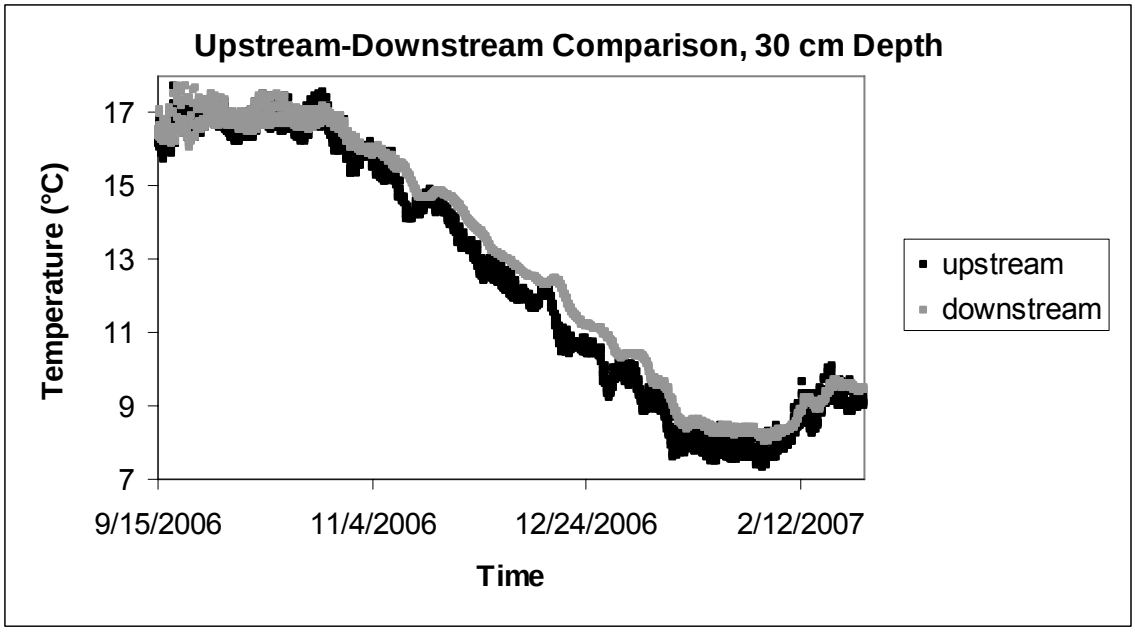


Figure 21. Observed temperatures from 30 cm depth, collected at the upstream (site 3803) and downstream (site 3809) edges of a riffle. Less diurnal fluctuation, higher wintertime temperature, and a phase lag in the day-to-day trend are present in the downstream temperature monitoring point.

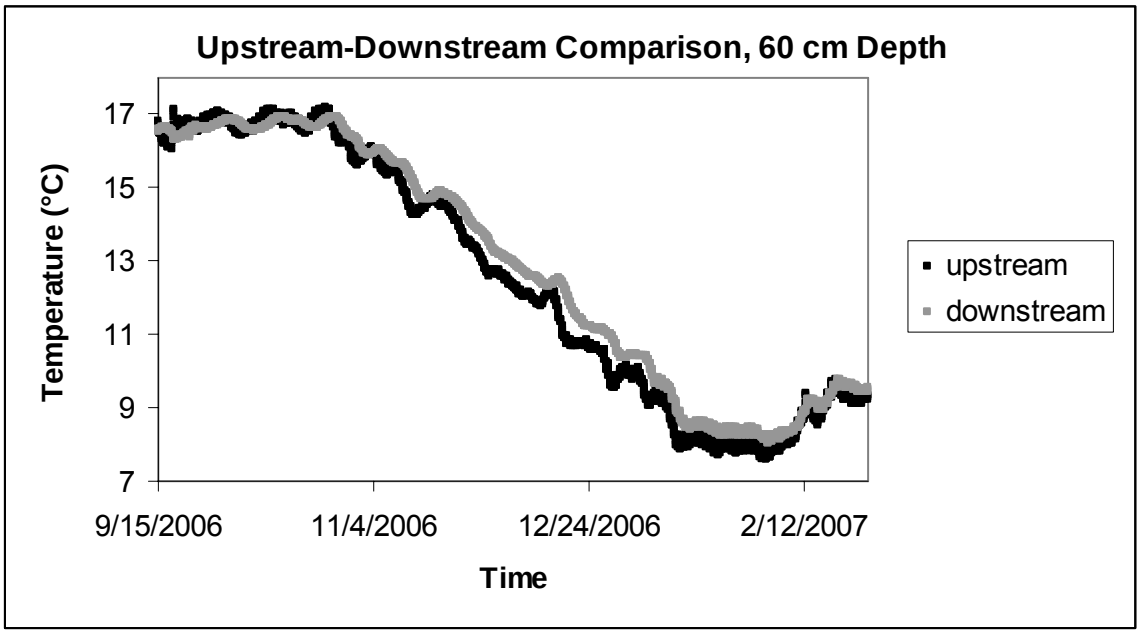


Figure 22. Observed temperatures from 60 cm depth, collected at the upstream (site 3803) and downstream (site 3809) edges of a riffle. Less diurnal fluctuation, higher wintertime temperature, and a phase lag in the day-to-day trend are present in the downstream temperature monitoring point.

Whether this heat transport is negligible, for the purpose of the vertical-dimension simulations presented earlier, depends on values of the product $q_x \cdot \partial T/\partial x$, compared to $q_z \cdot \partial T/\partial z$. Since we have a large array of temperature data, we compared the mean values of the spatial derivatives. Using temperatures collected in the same transect (Figure 28, 2006 monitoring sites), we estimated values of spatial derivatives. If $|\partial T/\partial z| >> |\partial T/\partial x|$, it may be reasonable to reduce heat transport problems, in these field conditions, to the vertical dimension only. We estimated values of $\partial T/\partial x$ and $\partial T/\partial z$ using cubic spline (smooth piecewise cubic polynomial) fits to the data, in each dimension. The mean of $|\partial T/\partial z|$ over a one-month period (July-August 2006) is shown in Table 3A and the mean of $|\partial T/\partial x|$ is shown in Table 3B. In general, the mean value of $|\partial T/\partial z|$ is around two orders of magnitude larger than the mean value of $|\partial T/\partial x|$. The smaller mean value of $|\partial T/\partial x|$ contributes toward smaller values of the longitudinal advective term in the heat transport equation, suggesting the vertical-dimension models presented earlier have some merit. However, to unequivocally conclude that the vertical model is valid, it would be necessary to construct and run a two-dimensional model, and compare results to those of the vertical-dimension models presented earlier. Overall, longitudinal transport exists and impacts the temperatures in shallow vertical profiles. Vertical-dimension modeling is a reasonable initial application of the heat tracer method in the shallow streambed, but a two-dimensional (longitudinal-vertical) model could be used to better account for all energy inputs and further evaluate the accuracy of vertical-dimension modeling.

**3A)** Mean $|\partial T/\partial z|$

| | x (m) = | 14.8 | 31.9 | 46.1 |
|---|---|---|---|---|
| z (m) = | 1.04 | 0.19 | 0.18 | 0.08 |
| | 1.16 | 0.14 | 0.16 | 0.08 |
| | 1.29 | 0.08 | 0.15 | 0.12 |
| | 1.39 | 0.05 | 0.19 | 0.15 |
| | 1.54 | 0.15 | 0.17 | 0.23 |
| | 1.69 | 0.15 | 0.38 | 0.36 |
| | 1.84 | 0.35 | 0.26 | 0.60 |
| | 1.99 | 0.52 | 1.58 | 1.47 |
| | 2.14 | 1.31 | 1.96 | 1.16 |
| | 2.19 | 1.92 | 1.18 | 1.12 |

**3B)** Mean $|\partial T/\partial x|$

| | x (m) = | 14.8 | 31.9 | 46.1 |
|---|---|---|---|---|
| z (m) = | 1.04 | 0.011 | 0.005 | 0.002 |
| | 1.16 | 0.011 | 0.006 | 0.002 |
| | 1.29 | 0.012 | 0.005 | 0.003 |
| | 1.39 | 0.012 | 0.004 | 0.002 |
| | 1.54 | 0.012 | 0.003 | 0.002 |
| | 1.69 | 0.010 | 0.003 | 0.003 |
| | 1.84 | 0.005 | 0.004 | 0.006 |
| | 1.99 | 0.005 | 0.010 | 0.010 |
| | 2.14 | 0.012 | 0.013 | 0.007 |
| | 2.19 | 0.012 | 0.011 | 0.008 |

**Table 3**. Mean values of spatial derivatives at nodes within the observation domain. $|\partial T/\partial z|$ mean values are typically around two orders of magnitude larger than $|\partial T/\partial x|$ mean values.

*Toward a Longitudinal-Vertical Model*

A longitudinal-vertical model of heat transport could be used to further evaluate flow in the shallow streambed, but was not part of this study. Tracing water flow using temperatures was performed by Cartwright (1974) and Woodbury and Smith (1988), through aquifer transects with lengths on the order of kilometers. However, longitudinal-vertical analysis has not been done on the scale of a single bedform (tens of meters). While VS2DH has been successfully used in transverse-vertical problems (e.g., Ronan et al, 1998), its options for boundary conditions are less conducive to a longitudinal-vertical model. The boundary condition for flow along the upper boundary is a water surface that slopes linearly downstream. In a numerical model of flow in a porous medium, this condition is implemented through a time-varying hydraulic head boundary condition that simulates the hydraulic gradient at the streambed surface. However, VS2DH simulates lateral gradients as piecewise constant boundary segments, producing spurious vertical flow (Figure 23).

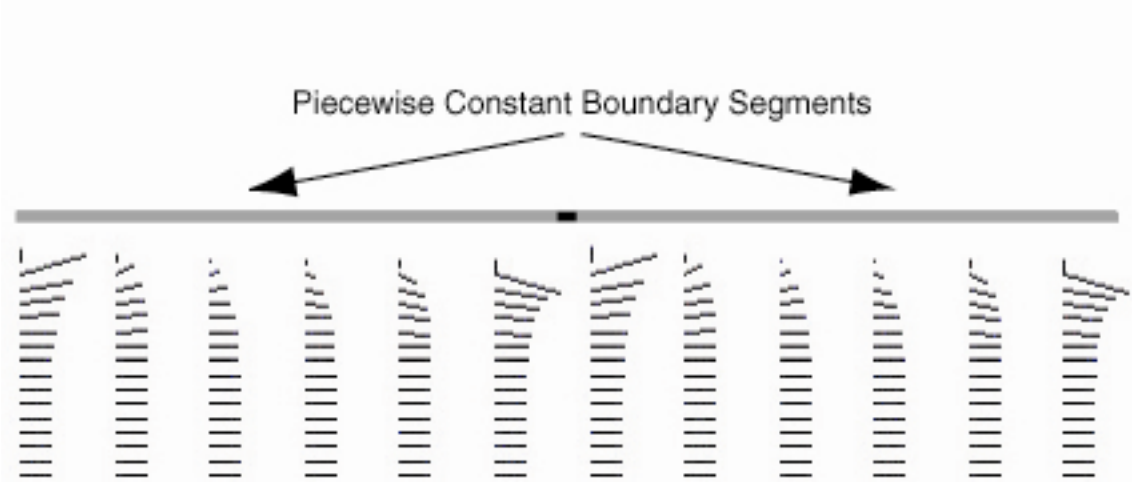


Figure 23. Flow vectors produced by VS2DH oscillate spuriously under piecewise constant boundary segments. Vectors shown were obtained by screen capture of the VS2DHI postprocessor.

Future work on a longitudinal-vertical model must address the need to accurately represent the flow condition along the upper boundary. Such a numerical model would be free of discontinuities in the gradient. Accurately representing the water surface along the upper boundary will allow researchers to then include conditions along other boundaries that drive non-horizontal flow. An artifact-free upper boundary is a necessary and remaining problem to address in any attempt to model flow and heat transport in a bedform-scale longitudinal-vertical transect.

# Chapter 6

# CONCLUSIONS

Despite the success of many of our vertical-dimension simulations, two-dimensional treatment of these problems is appropriate and should improve the quality of results. Indications include 1) inability of the vertical-dimension model to fully reproduce temperature conditions at site 3606, 2) the demonstrated effect of longitudinal flow causing later phase in vertically-simulated temperatures, and 3) the estimation that the mean value of $|\partial T/dx|$ is generally about two orders of magnitude less than the mean value of $|\partial T/dz|$, which is perhaps negligible in some cases but nevertheless indicates that longitudinal heat transport occurs. Development of a model able to perform longitudinal-vertical simulations of water flow and heat transport, with accurate flow boundary conditions, would more completely account for heat transport in the shallow streambed.

Even with the problem of longitudinal heat transport unresolved, in many cases, simulation of coupled water flow and heat transport in the vertical dimension has been used to obtain reasonable simulated-observed temperature matches. Simulations suggest hydraulic conductivity varies by site and that it may also vary vertically in the streambed. The seepage and hydraulic conductivity used to produce these matches are useful parameters to quantify for the purpose of characterizing flow through the streambed and its effects on salmonid spawning habitat. This indicates that shallow temperature profiles are a useful tool for streambed research in large, gravel-bed streams.

# REFERENCES

Anderson MP. 2005. Heat as a ground water tracer. Ground Water 43: 951-968. DOI 10.1111/j.1745-6584.2005.00052.x.

Bartolino JR. 2003. The Rio Grande—competing demands for a desert river. In *Heat as a tool for studying the movement of ground water near streams*, Stonestrom DA, Constantz J (eds). U.S. Geological Survey, Circular 1260: Reston; 7-16.

Bartolino JR, Niswonger RG. 1999. Numerical simulation of vertical ground-water flux of the Rio Grande from ground-water temperature. U.S. Geological Survey Water-Resources Investigations Report 99-4212.

Bravo HR, Feng J, Hunt RJ. 2002. Using groundwater temperature data to constrain parameter estimation in a groundwater flow model of a wetland system. *Water Resources Research* **38**: 1153. DOI 10.1029/2000WR000172.

Bear, J. 1972. Dynamics of fluids in porous media. American Elsevier: New York; 125-126.

Bredehoeft JD, Papadopulos IS. 1965. Rates of vertical groundwater movement estimated from the Earth's thermal profile. *Water Resources Research* **1**: 325-328.

Bundschuh J. 1993. Modeling annual variations of spring and groundwater temperatures associated with shallow aquifer systems. *Journal of Hydrology* **142**: 427-444.

Cardenas MB, Zlotnik VA. 2003. A simple constant-head injection test for streambed hydraulic conductivity estimation. *Ground Water* **41**: 867-871.

Chen X. 2000. Measurement of streambed hydraulic conductivity and its anisotropy. *Environmental Geology* **39**: 1317-1324.

Conlon T, Lee K, Risley J. 2003. Heat tracing in streams in the central Willamette Basin, Oregon. In *Heat as a tool for studying the movement of ground water near streams*, Stonestrom DA, Constantz J (eds). U.S. Geological Survey, Circular 1260: Reston; 29-34.

Constantz J, Cox MH, Su GW. 2003. Comparison of heat and bromide as ground water tracers near streams. *Ground Water* **41**: 647-656.

Constantz J, Murphy F. 1991. The temperature dependence of ponded infiltration under isothermal conditions. *Journal of Hydrology* **122**: 119-128.

Constantz J, Stewart AE, Niswonger R, Sarma L. 2002. Analysis of temperature profiles for investigating stream losses beneath ephemeral channels. *Water Resources Research* **38**: 1316. DOI 10.1029/2001WR001221.

Constantz J, Stonestrom DA. 2003. Heat as a tracer of water movement near streams. In *Heat as a tool for studying the movement of ground water near* streams, Stonestrom DA, Constantz J (eds). U.S. Geological Survey, Circular 1260: Reston; 1-6.

Constantz J, Thomas CL. 1996. The use of streambed temperature profiles to estimate the depth, duration, and rate of percolation beneath arroyos. *Water Resources Research* **32**: 3597-3602.

Cartwright K. 1974. Tracing shallow groundwater systems by soil temperatures. *Water Resources Research* **10**: 847-855.

Fetter CW. 1994. Applied Hydrogeology. Prentice Hall: Upper Saddle River, New Jersey; 75.

Healy RW, Ronan AD. 1996. Documentation of computer program VS2DH for simulation of energy transport in variably saturated porous media—modification of the U.S. Geological Survey's computer program VS2D. *U.S. Geological Survey Water-Resources Investigations Report* 96-4230.

Hoffmann JP, Blasch KW, Ferre TP. 2003. Combined use of heat and soil-water content to determine stream/ground-water exchanges, Rillito Creek, Arizona. In *Heat as a tool for studying the movement of ground water near streams*, Stonestrom DA, Constantz J (eds). U.S. Geological Survey, Circular 1260: Reston; 47-55.

Hopmans JW, Simunek J, Bristow KL. 2002. Indirect estimation of soil thermal properties and water flux suing heat pulse probe measurements: geometry and dispersion effects. Water Resources Research 38: 1006. DOI 10.1029/2000WR000071.

Horner TC, Titus R, Brown M. 2003. Phase 3 gravel assessment on the Lower American River. California Dept. of Fish and Game, Stream Evaluation Program Technical Publication Series: Sacramento; 93 p.

Hsieh PA, Wingle W, Healy RW. 2000. VS2DI—A graphical software package for simulating fluid flow and solute or energy transport in variably saturated porous media. *U.S. Geological Survey Water-Resources Investigations Report* 99-4130.

Keery J, Binley A, Crook N, Smith JWN. 2007. Temporal and spatial variability of groundwater-surface water fluxes: development and application of an analytical method using temperature time series. *Journal of Hydrology* **336**: 1-16.

Kondolf GM, Wolman MG. 1993. The sizes of salmonid spawning gravels. *Water Resources Research* **29**: 2275-2285.

Landon MK, Rus DL, Harvey FE. 2001. Comparison of instream methods for measuring hydraulic conductivity in sandy streambeds. *Ground Water* **39**: 870-885.

Lapham WW. 1989. Use of temperature profiles beneath streams to determine rates of vertical ground-water flow and vertical hydraulic conductivity. U.S. Geological Survey Water Supply Paper 2337: Denver; 44 p.

Lee DR, Cherry JA. 1978. A field exercise on groundwater flow using seepage meters and mini-piezometers. Journal of Geological Education **27**: 6-10.

Lisle TE. 1989. Sediment transport and resulting deposition in spawning gravels, north coastal California. *Water Resources Research* **25**: 1303-1319.

McEwan DR. 2001. Central Valley Steelhead. In *Contributions to the biology of Central Valley salmonids*, Brown RL (ed). California Dept. of Fish and Game, Fish Bulletin No. 179.1: Sacramento; 1-44.

Merz JE, Setka JD. 2004. Evaluation of a spawning habitat enhancement site for Chinook salmon in a regulated California river. *North American Journal of Fisheries Management* **24**: 397-407.

Niswonger RG, Prudic DE. 2003. Modeling heat as a tracer to estimate streambed seepage and hydraulic conductivity. In *Heat as a tool for studying the movement of ground water near streams*, Stonestrom DA, Constantz J (eds). U.S. Geological Survey, Circular 1260: Reston; 81-89.

Packman AI, Bencala KE. 2000. Modeling Surface-Subsurface Hydrological Interactions. In *Streams and Ground Waters*, Jones JB, Mulholland PJ (eds). Academic Press: San Diego, 46-77.

Pollard RA. 1955. Measuring seepage through salmon spawning gravel. *Journal of Fisheries Research Board of Canada* **12**: 706-741.

Ronan AD, Prudic DE, Thodal CE, and Constantz J. 1998. Field study and simulation of diurnal temperature effects on infiltration and variably saturated flow beneath an ephemeral stream. *Water Resources Research* **34**: 2137-2153.

Silliman SE, Booth DF. 1993. Analysis of time-series measurements of sediment temperature for identification of gaining vs. losing portions of Juday Creek, Indiana. *Journal of Hydrology* **146**: 131-148.

Smith L, Chapman DS. 1983. On the thermal effects of groundwater flow. 1. Regional scale systems. *Journal of Geophysical Research* **88**: 593-608.

Sowden TK, Power G. 1985. Prediction of Rainbow Trout Embryo Survival in Relation to Groundwater Seepage and Particle Size of Spawning Substrates. *Transactions of the American Fisheries Society* **114**: 804-812.

Stallman RW. 1965. Steady one-dimensional fluid flow in a semi-infinite porous medium with sinusoidal surface temperature. *Journal of Geophysical Research* **70**: 2821-2827.

Stonestrom DA, Constantz J (eds). 2003. Heat as a tool for studying the movement of ground water near streams. *U.S. Geological Survey Circular 1260*: Reston, 96 p.

Su GW, Jasperse J, Seymour D, and Constantz J. 2004. Estimation of hydraulic conductivity in an alluvial system using temperatures. *Ground Water* **42**: 890-901.

Suzuki S. 1960. Percolation measurements based on heat flow through soil with special reference to paddy fields. *Journal of Geophysical Research* **65**: 2883-2885.

Taniguchi M. 1993. Evaluation of vertical groundwater fluxes and thermal properties of aquifers based on transient temperature-depth profiles. *Water Resources Research* **29**: 2021-2026.

Thibodeaux LJ, Boyle JD. 1987. Bedform-generated convective transport in bottom sediment. *Nature* **325**: 341-343.

Turnpenny AWH, Williams R. 1980. Effects of sedimentation on the gravels of an industrial river system. *Journal of Fish Biology* **17**: 681-693.

Vyverberg K, Snider B, and Titus RG. 1997. Lower American River Chinook salmon spawning habitat evaluation October 1994. California Dept. of Fish and Game Environmental Services Division, Technical Report 97-2: Sacramento; 112 p.

Williams JG. 2001. Chinook salmon in the lower American River, California's largest urban stream. In *Contributions to the biology of Central Valley salmonids*, Brown RL (ed). California Dept. of Fish and Game, Fish Bulletin No. 179.2: Sacramento; 1-38.

Williams JG. 2006. Central Valley salmon: A perspective on Chinook and Steelhead in the Central Valley of California. *San Francisco Estuary and Watershed Science* **4**: Article 2.

Wroblicky GJ, Campana ME, Valett HM, Dahm CN. 1998. Seasonal variation in surface-subsurface water exchange and lateral hyporheic area of two stream-aquifer systems. *Water Resources Research* **34**: 317-328.

Woodbury AD, Smith L. 1988. Simultaneous inversion of hydrogeologic and thermal data: 2. Incorporation of thermal data. *Water Resources Research* **24**: 356-372.

Zamora, C. 2006. Estimating rates of exchange across the sediment/water interface in the lower Merced River, CA. Unpublished M.S. thesis. California State University, Sacramento.